Ann. Rev. Nucl. Part. Sci. 1978. 28:33–113

SYNCHROTRON RADIATION RESEARCH

*5592

Herman Winick and Arthur Bienenstock
Stanford Synchrotron Radiation Laboratory, Stanford, California 94305

CONTENTS

1 INTRODUCTION

Synchrotron radiation, the electromagnetic radiation emitted by relativistic electrons traveling in curved paths, opens new possibilities in research and technology that have already produced important results and are

0066-4243/78/1201-0033$01.00

expected to have even greater impact in the future. With the development of high energy electron synchrotrons and storage rings for elementary particle research, very powerful sources of synchrotron radiation are now available and are extensively used for synchrotron radiation research, largely in a symbiotic manner with the high energy physics programs. In more than twenty laboratories throughout the world, the broad spectrum of intense, collimated, and polarized x rays and ultraviolet radiation is being used for experiments in structural biology, catalytic chemistry, surface physics, solid state physics, and many other areas, including applications to technology such as microstructure replication and x-ray topography.

Although synchrotron radiation research began in the early 1960s, most of the work until 1974 was concentrated in the ultraviolet part of the spectrum, and almost all the sources were synchrotrons. Starting in about 1974, a new generation of multi-GeV storage rings became available (SPEAR, DORIS, VEPP-3). These provide higher intensity, a more constant spectrum, and greater stability than synchrotrons.

The first major synchrotron radiation research facility utilizing a multi-GeV storage ring was the Stanford Synchrotron Radiation Laboratory (SSRL), which began operation in May 1974. The results from SSRL and from the other multi-GeV storage rings conclusively showed the enormous capability of synchrotron radiation from 150 eV to 35 keV as produced by a storage ring. Earlier results from smaller storage rings at Wisconsin and Orsay had already proven the case for lower photon energies.

As published work in this new energy region began to appear, an extremely large growth in user interest occurred. For example, at SSRL the number of active research proposals in January 1978 exceeded 200 and has approximately doubled each year for the last three years. Evaluation of national needs has prompted several countries (England, Germany, Japan, and the US) to construct new storage rings dedicated only to synchrotron radiation research and greatly to increase the programs on existing machines.

The unique properties of synchrotron radiation (markedly different both quantitatively and qualitatively from other radiation sources) are, of course, responsible for these developments. The most important characteristic of synchrotron radiation is the high and extremely stable intensity over a broad bandwidth. This frees researchers from working only at the discrete lines available from conventional sources in the ultraviolet (UV) and x-ray part of the spectrum. As a continuum x-ray source for example, synchrotron radiation makes available more than 100,000 times higher flux than the most powerful rotating anode x-ray generators. This has

led, among other results, to the development of the technique known as Extended X-Ray Absorption Fine Structure (EXAFS) from an interesting laboratory curiosity to a powerful analytic tool for the determination of local atomic environment in complex systems. Spectra that took two weeks to acquire using powerful conventional sources are now routinely obtained in 20 minutes—and with improved signal-to-noise ratio. The widely applicable technique (it can be used on gases, liquids, and solids) has, for example, already contributed significantly to the understanding of amorphous materials, biological enzymes, industrial catalysts, phase transitions, and dilute impurities.

The high intensity also facilitates structural studies by large- and small-angle x-ray diffraction. A particularly exciting prospect is the ability to do dynamic structural studies to elucidate nerve and muscle functions, crystal growth, and mechanical failure processes on a millisecond time scale.

The extreme collimation (the radiation is emitted in a cone with an opening angle <1 mrad for storage rings with energy >1 GeV) means that highly monochromatic beams can be produced using gratings and crystals, permitting high resolution studies of absorption edges, core levels, etc. This feature also permits the use of soft x-ray lithography for the fabrication of microstructures such as memory devices, Josephson junctions, and integrated circuits. At soft x-ray wavelengths (10–50 Å), diffraction effects are much reduced compared to visible light. Thus, the naturally collimated, essentially parallel rays can be used to replicate the pattern of a mask (with features as small as 1000 Å or less) onto a silicon wafer without penumbral blurring. Future developments in this area are likely to have a major impact on very-large-scale integration (VLSI) technology.

Because electrons are not uniformly distributed around the perimeter of a storage ring, but rather are bunched, the radiation has a sharply pulsed time structure. In the SPEAR storage ring, for example, the pulses are of ~ 300 psec duration with a repetition rate of 1.28 MHz. This feature is used increasingly for lifetime measurements in atomic and molecular systems and may facilitate the pumping of an x-ray laser. In the future, with the increased intensity that will become available, it is likely that these timing properties will be used to extend dynamical structural studies to a submicrosecond time scale.

In storage rings, the high vacuum environment and small source size of the electron beam have enabled experimenters to image the source onto extremely small samples for studies of fresh surfaces prepared in situ in ultrahigh vacuum sample chambers. The measurement of the energy and angular distribution of photoelectrons produced by a tunable photon

beam incident on clean surfaces and on surfaces covered with adsorbed gases is a very powerful technique for understanding electronic structure and surface processes such as oxidation, catalysis, and corrosion.

The very high polarization of synchrotron radiation (almost 100% linear polarization in the median plane, 75% integrated over all vertical angles) is an important feature that can be used to advantage in many measurements such as scattering and fluorescence experiments, including resonant nuclear (Mössbauer) scattering. For example, in trace element fluorescence measurements, increased sensitivity results from the decreased background scattering in the direction of polarization. Polarization has also made it possible to observe quantum beats in the fluorescence from magnetically oriented atoms.

Any one of the above-described characteristics would make synchrotron radiation an important experimental tool. The combination of all makes it an ideal source for an extremely broad, interdisciplinary range of spectroscopic and structural studies.

Almost all present sources are primarily operated for high energy physics purposes. Considerably higher intensity and brightness will be available when these machines become available as dedicated synchrotron radiation sources and when new dedicated synchrotron radiation sources, now in construction, become operational. Furthermore, all of the research to date has made use of the radiation produced in the ring bending magnets, where the magnetic field is typically $\lesssim 12$ kG. Over the next few years, it is likely that special insertions (such as high field wiggler magnets, multipole interference wigglers and possibly free electron lasers) will significantly extend experimental capabilities by enhancing and modifying the normal synchrotron radiation spectrum.

Similarly, in the experimental utilization of the radiation, it is likely that new designs for UV and x-ray optical systems, monochromators and detectors will result in instruments better matched to the properties of synchrotron radiation, and this will result in a further increase in experimental capability.

In this review, we describe the sources and properties of synchrotron radiation and cover some of the many scientific and technological applications and specific research results from laboratories throughout the world. In a review of this size, we cannot properly cover all of the important scientific accomplishments using synchrotron radiation. We have attempted to describe briefly a fairly large number of applications and cover a few in more detail. Most of the examples used will be taken from work at the Stanford Synchrotron Radiation Laboratory because of the association of the authors with this laboratory and because, at present, this is the laboratory with the broadest program of research in the UV

and x-ray spectral regions. We apologize in advance for being unable to mention, because of space limitations, some of the excellent results obtained at SSRL and elsewhere.

2 SOURCES OF SYNCHROTRON RADIATION—SYNCHROTRONS AND STORAGE RINGS

With the development of electron synchrotrons (since the 1940s) and storage rings (since the 1960s) for high energy physics research, intense sources of synchrotron radiation have become available. For the high energy physicists this radiation is generally considered to be a nuisance causing background in detectors, requiring water cooling of vacuum chambers, and large rf systems to replenish the lost energy. However, as remarked by W. K. H. Panofsky, "The background for one experiment is the signal for another."

Most of the machines now used as synchrotron radiation sources were constructed and are still used primarily for high energy physics purposes. This situation is changing with the design and construction of several storage rings to be used as dedicated synchrotron radiation sources and the transition to dedicated synchrotron radiation operation on existing machines (the parasites are consuming the hosts).

The most capable source of synchrotron radiation is the storage ring. Figure 1 shows the basic features of an electron storage ring designed as a synchrotron radiation source. A closed continuous high vacuum chamber threads through various ring elements including: (*a*) bending magnets that bend the electrons in a circle and produce synchrotron radiation (only one magnet is shown); (*b*) special insertions (optional), such as the wiggler magnets shown in the drawing, to produce particularly intense or enhanced radiation; (*c*) an rf cavity and associated power supply, which replenishes the energy lost by the electron beam into synchrotron radiation; (*d*) vacuum pumps to evacuate the chamber; and (*e*) an inflector that permits electrons from a separate accelerator (not shown) to be injected.

In a properly designed storage ring, large currents of electrons (hundreds of milliamperes) can be accumulated within several minutes and adjusted within several additional minutes to any desired energy within range of the ring. Injection can be below the operating energy, with the storage ring then used briefly as a slow accelerator to increase the energy. Injection at the operating energy is quicker, provides the highest stored beam current, and maximizes experimental running time, but, of course, requires a more powerful injector accelerator.

With storage ring average pressure in the 10^{-9}-Torr range, electron

beam encounters with residual gas molecules are sufficiently rare that the stored current decays with a time constant of two to twenty hours and in some cases even longer. The synchrotron light intensity as well as the spectrum and other source properties are, therefore, quite stable over long periods of time in a storage ring.

A synchrotron is quite similar in some ways; it consists of a roughly circular ring of magnets, vacuum chamber, and other components similar to the storage ring. The similarity is so close that a single ring could be made to operate as a synchrotron and as a storage ring as was done at the Cambridge Electron Accelerator (CEA) (1). However, a synchrotron is designed to accelerate rapidly (in ~ 10 msec) groups of $\sim 10^{11}$ electrons from a low injection energy to a maximum energy some 10–100 times higher. At the high energy the electrons strike an internal target or are extracted to strike an external target. The process of injection and acceleration of a new group of electrons then starts over again, repeating at 50–60 Hz.

Therefore, in synchrotrons the electron energy and consequently the synchrotron radiation spectrum are not constant. Also, the electron beam current, position, and cross-sectional area vary within an accelera-

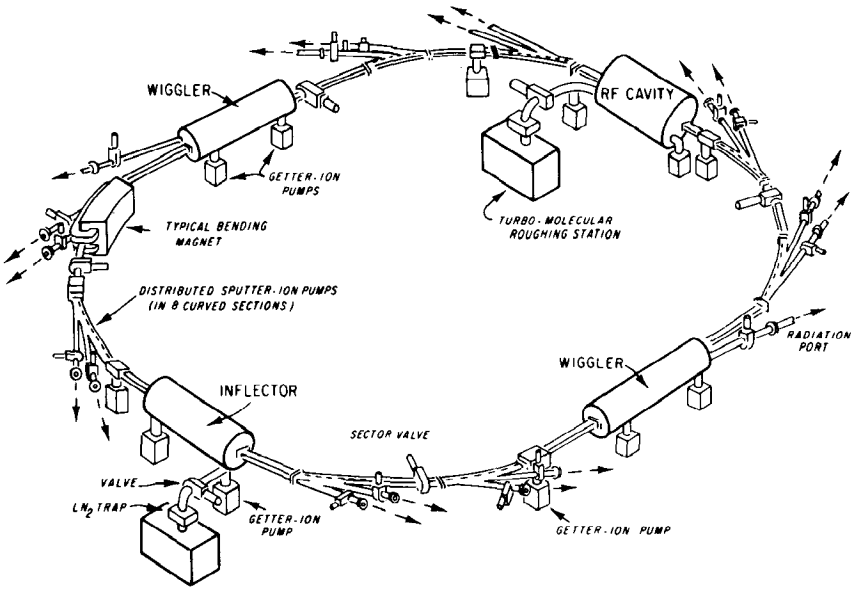

Figure 1 Artist conception of an electron storage ring designed as a source of synchrotron radiation. Not shown is the injector accelerator. Courtesy of J. Godell, Brookhaven National Laboratory.

tion cycle and from one cycle to the next. Furthermore, the large amount of high energy radiation near electron synchrotrons requires that synchrotron radiation experiments be totally enclosed in shielded areas, remotely controlled, and generally less accessible than those performed on a storage ring.

In spite of these difficulties, much synchrotron radiation research has been done with electron synchrotrons because they produce high photon flux extending to very high energy and, historically, they were available before storage rings.

Tangential ports permit the synchrotron radiation to leave the vacuum enclosure and travel to the experiments. One such port can accept sufficient radiation (10–50 mrad of arc) to serve more than one experiment simultaneously. Figure 2 shows how a single tangential port may be split and mirrors, gratings, and crystals used to serve several simultaneous experimental stations. Detailed descriptions of synchrotron radiation beam lines and research facilities are available, including descriptions of the facilities at Hamburg (2, 3), Orsay (4), and Stanford (5, 6).

3 HISTORY OF THEORETICAL AND EXPERIMENTAL WORK

Consideration of the radiation from accelerated charges goes back to the 19th century, and the work of Liénard (7) for example. Further work during the next fifty years was done by many authors (8–13). A useful bibliography (14) of works relating to synchrotron radiation gives additional references through 1974.

Among the first to be concerned about radiation effects in circular electron accelerators were Ivanenko & Pomeranchuk (10) and Blewett (12). Synchrotron radiation was first observed (accidentally) at the General Electric 70-MeV synchrotron in 1947.

Extensive theoretical work has been done by Sokolov and co-workers (15–18), Schwinger (13), and others. Quantum mechanical effects were shown to be negligible in practical cases. The theory is reviewed in the textbook by Jackson (19).

Experimental investigations on the properties of the radiation were carried out by Pollack and co-workers (20) using the General Electric 70-MeV synchrotron, by several groups (21–23) using the 250-MeV synchrotron at the Lebedev Institute in Moscow, by Corson (24) and Tomboulian and co-workers (25–27) using the Cornell 300-MeV synchrotron, by Codling & Madden (28) using the 180-MeV synchrotron at the National Bureau of Standards (NBS) in Washington, DC, and by

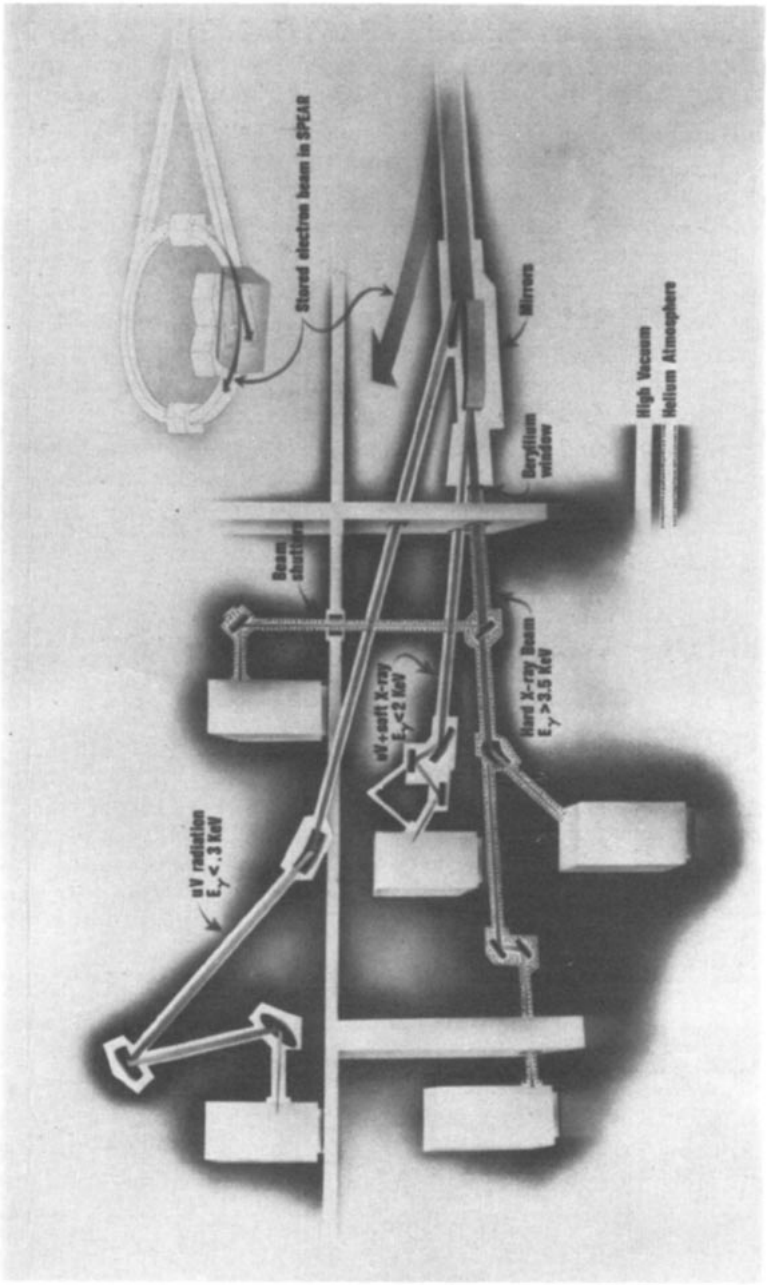

Figure 2 Artist conception of the first beam line implemented in 1974 at the Stanford Synchrotron Radiation Project. Courtesy of W. Zawojski, SLAC.

Haensel and co-workers (29) using the 6-GeV synchrotron in Hamburg. These studies verified the basic theoretical predictions regarding intensity, angular distribution, spectral distribution, polarization, etc, and also provided practical data and experience in the use of radiation.

A research program using synchrotron radiation was initiated in 1961 at the Frascati synchrotron, in 1963 at the NBS and Tokyo synchrotrons, and in 1966 at the Hamburg synchrotron. By 1972, programs were also underway at synchrotrons in Bonn, Yerevan, Glasgow, Lund, Moscow, and other locations. In most of these cases, the primary function of the synchrotron was high energy physics research.

The superior properties of the synchrotron radiation produced by a storage ring (e.g. constant spectral distribution, stable intensity) were first made available at the 240-MeV ring (30) at the University of Wisconsin, which began producing ultraviolet radiation in 1968 as a dedicated synchrotron radiation source. Larger storage rings extended these desirable characteristics to higher photon energy. In 1971, a synchrotron radiation program in the ultraviolet part of the spectrum was started on the 540-MeV ring (4) in Orsay, France. The x-ray part of the spectrum was opened in 1972 at the Cambridge Electron Accelerator (CEA) in Massachusetts, operating as a storage ring at 3 GeV (31). The Wisconsin and Orsay machines continue in operation with the French machine now also fully dedicated to synchrotron radiation research. The CEA ceased operation for high energy physics and synchrotron radiation research in 1973.

By 1972, the potential of synchrotron radiation as a multidisciplinary research tool had attracted the attention of many scientists. The proceedings of a symposium (32) on synchrotron radiation research held at Brookhaven in 1972 give an overview of the field and its prospects as seen at that time. In late 1972, a panel was formed by the National Science Foundation in the USA to study three proposals for synchrotron radiation research facilities. These proposals were for: (*a*) construction of a new 1.76-GeV electron storage ring at the University of Wisconsin to be dedicated to synchrotron radiation research; (*b*) dedication of the CEA storage ring at Harvard University to synchrotron radiation research; and (*c*) construction of the Stanford Synchrotron Radiation Project (SSRP) utilizing synchrotron radiation produced during high energy physics colliding-beam operation of the storage ring SPEAR at the Stanford Linear Accelerator Center (SLAC).

The panel concluded that synchrotron radiation offered interesting research prospects for radiation extending all the way into the short wavelength x-ray region. The third alternative, SSRP, (now SSRL) was authorized as the least costly way to evaluate these prospects.

SSRP (6, 33) was funded in June 1973 and began research operation on five experimental stations, each with a monochromator, in May 1974. This was the first time that synchrotron radiation from a multi-GeV storage ring became available to a large community of users. Within about a year, programs were also begun on the VEPP-3 storage ring in Novosibirsk, USSR, and the DORIS storage ring in Hamburg, Germany. The results obtained from the extended spectral range on these newly available large rings, plus continued results from smaller storage rings and synchrotrons throughout the world, have convinced scientists that synchrotron radiation is a powerful tool for basic and applied research in a large variety of fields such as atomic physics, structural biology, and microfabrication. A comprehensive report (5) on research with synchrotron radiation at SSRP and the prospects for future use of a multi-GeV storage ring was completed in 1976.

Compared with the cautious optimism about the usefulness of synchrotron radiation in 1973, by 1975 the capability was clearly proven, and the enormous increase in user demand created an urgent need to provide more experimental facilities. In 1975, the British, after completing a study of their national needs for synchrotron radiation facilities (34), authorized construction of the world's first multi-GeV storage ring as a dedicated source. Since then, additional proposals for dedicated sources have been made in Japan, the Netherlands, the Soviet Union, the United States, and elsewhere. Many of these have since been authorized and are now under construction. The present status is summarized in Tables 1–4.

Storage rings designed as dedicated sources of synchrotron radiation should offer advantages over machines designed for high energy physics purposes. These include ability to accommodate a larger number of synchrotron radiation beam lines and higher source point brightness due to reduced electron beam emittance. Design reports such as those produced at Brookhaven (35) and in the Netherlands (36) give more detailed considerations.

In early 1976, another panel was formed in the US to assess the national need for facilities dedicated to the production of synchrotron radiation. The panel projected the number of experimental stations that would be needed by 1986 to accommodate those scientists expected to be using synchrotron radiation in their research programs. The results of this projection are given in Table 5 taken from the panel report (37).

The major recommendation of the August 1976 panel report (37) was that "an immediate commitment be made to construct new dedicated national facilities and to expand existing facilities so that optimized XUV and x-ray capabilities are provided . . ." (p. 5).

The case was so compelling that the recommendations of the panel

were almost immediately included in budget submissions by government agencies in 1976 and subsequently approved by Congress in 1977. Under construction now in the United States are two dedicated storage rings at Brookhaven National Laboratory (35), one at the University of Wisconsin, and one colliding-beam storage ring at Cornell University (38) to be also used for synchrotron radiation research. In addition, a major

Table 1 Synchrotron radiation sources—storage rings in operation—February 1978

Machine, location	E (GeV)	I (mA)	R (m)	ε_c (keV)	Remarks
VEPP-4	7	10	16.5	46.1	Initial operation at 4.5 GeV
Novosibirsk, USSR	4.5		(18.6)	(10.9)	(from 8-kG wiggler part of magnet lattice)
DORIS	2.2	300	12.1	1.95	
Hamburg, Germany	5.0	50		22.9	
SPEAR	2.25	300(10)	12.7	2.0	(colliding beam
Stanford, US	4.0	100(35)		11.1	current limits)
VEPP-3	2.25	100	6.15	4.2	Operation to 3 GeV is possible
Novosibirsk, USSR			(2.14)	(11.8)	(from 35-kG wiggler planned)
DCI					
Orsay, France	1.8	500	4.0	3.63	
ADONE					
Frascati, Italy	1.5	60	5.0	1.5	Synchrotron radiation lines in construction
			(2.8)	(2.7)	(from 18-kG wiggler planned)
VEPP-2M					
Novosibirsk, USSR	0.67	100	1.22	0.54	
ACO					
Orsay, France	0.54	100	1.1	0.32	Dedicated[a]
SOR Ring					
Tokyo, Japan	0.40	250	1.1	0.130	Dedicated[a]
TANTALUS I					
Wisconsin, US	0.24	200	0.64	0.048	Dedicated[a]
SURF II					
Washington, DC, US	0.25	25	0.84	0.036	Dedicated[a]
N-100					
Karkhov, USSR	0.10	25	0.50	0.004	

[a] Dedicated machines are used only for synchrotron radiation research. Other machines are used for both high energy physics research and synchrotron radiation research.

expansion of facilities is underway at SSRL (5, 39), and SPEAR is expected to be a dedicated source for 50% of the operations time starting in about 1980.

In 1977, a report surveying European synchrotron radiation facilities and needs for the future was published (40). The report concluded (p. 1)

Table 2 Synchrotron radiation sources—storage rings in construction—February 1978

Machine, location expected completion date	E (GeV)	I (mA)	R (m)	ε_c (keV)	Remarks
PETRA[a]	18	18	192	67.4	
Hamburg, Germany	15	80		39.0	
1978	10	50		11.6	
PEP[a]	18	10	165.5	78	
Stanford, US	15	55		45.2	
1979	10	35		13.4	
	12	45	(23.6)	(163)	(from 17-kG wiggler part of PEP lattice)
CESR[a]	8	100	32.5	35	Synchrotron radiation
Cornell, US	4	50	32.5	4.4	facility planned
1979					
PHOTON FACTORY	2.5	500	8.33	4.16	Dedicated
Tsukuba, Japan			(1.67)	(20.5)	(for a 50-kG wiggler)
1981					
NSLS					
Brookhaven National	2.5	500	8.17	4.2	Dedicated
Lab, US			(1.67)	(20.5)	(for a 50-kG wiggler)
1981					
SRS	2.0	500	5.55	3.2	Dedicated
Daresbury, UK			(1.33)	(13.3)	(from 50-kG wiggler
1979					planned)
ALADDIN					
Wisconsin, US	1.0	500	2.08	1.70	Dedicated
1980					
BESSY					
Berlin, West Germany					
1982	0.80	500	1.83	0.62	Dedicated; industrial use planned
NSLS					
Brookhaven National	0.70	500	1.90	0.40	Dedicated
Lab, US					
1981					

[a] PETRA, PEP, and CESR will operate over a range of energies. Examples of expected characteristics are given.

Table 3 Synchrotron radiation sources—storage rings proposed as of February 1978

Machine, location	E (GeV)	I (mA)	R (m)	ε_c (keV)	Remarks
ERSINE					
Yerevan, USSR	2.5	500	5.21	6.67	Dedicated
PAMPUS					
Amsterdam, Netherlands	1.5	500	4.17	1.80	Dedicated (2 GeV operation possible)
IPP					
Moscow, USSR	1.35	100	2.5	2.2	Dedicated (2 GeV also considered)
CSRL					
Canada	1.2	100	3.1	1.33	Dedicated
Electrotechnical Lab Tokyo, Japan	0.6	100	2.0	0.24	Dedicated

Table 4 Synchrotron radiation sources—synchrotrons in operation—February 1978

Machine, location	E (GeV)	I (mA)	R (m)	ε_c (keV)
DESY				
Hamburg, Germany	7.5	10–30	31.7	29.5
ARUS				
Yerevan, USSR	4.5	1.5	24.6	8.22
BONN I				
Bonn, Germany	2.5	30	7.6	4.6
SIRIUS				
Tomsk, USSR	1.36	15	4.23	1.32
INS-ES				
Tokyo, Japan	1.3	30	4.0	1.22
PAKHRA				
Moscow, USSR	1.3	300	4.0	1.22
LUSY				
Lund, Sweden	1.2	40	3.6	1.06
FIAN, C-60				
Moscow, USSR	0.68	10	1.6	0.44
BONN II				
Bonn, Germany	0.5	30	1.7	0.16

Table 5 Minimum predicted growth in synchrotron radiation facilities

	Present (Dec. 1976)		1986	
Use	Users	Stations	Users	Stations
X-Radiation	85	7	675	~60
XUV	120	16	480	~40

that "There will be a large discrepancy between the number of scientists who wish to use synchrotron radiation and the number of stations available on existing or proposed machines." The report stated (p. 1) that "A large effort to build a dedicated hard x-ray storage ring and appropriate advanced instrumentation with a design which goes beyond that of present day projects is recommended. This machine should be operational by 1985."

4 PROPERTIES OF SYNCHROTRON RADIATION

The most important properties of synchrotron radiation from an experimental point of view are the total power radiated, the angular distribution, the spectral distribution, and the polarization. Other properties of the radiation depend on the design of the particular machine. These include the pulsed time structure and the optical properties of the source point (i.e. electron beam size and divergence convoluted with the angular distribution of the emitted radiation).

We briefly discuss these topics in this section. More detailed treatments are given elsewhere (13, 19, 26, 41, 42). Particularly detailed tables and graphs describing the spectrum, angular distribution, and polarization functions are given by Green (43), who also gives an approximate treatment of the optical properties of the source. Elegant field plots showing the directionality of the synchrotron radiation from a charge in circular motion are given by Tsien (44).

4.1 *Power Radiated*

The Larmor formula (45) for power radiated by a single nonrelativistic accelerated charged particle is

$$P = \frac{2}{3}\frac{e^2}{c^3}\left|\frac{d\mathbf{v}}{dt}\right|^2 = \frac{2}{3}\frac{e^2}{m^2c^3}\left|\frac{d\mathbf{p}}{dt}\right|^2. \qquad 1.$$

For a particle in circular motion with radius of curvature ρ the relativistic generalization of the Larmor formula is

$$P = \frac{2}{3}\frac{e^2 c}{\rho^2}\beta^4\left[\frac{E}{mc^2}\right]^4. \qquad 2.$$

The energy loss per turn can be readily obtained from Equation 2.

$$\Delta E = P \cdot \frac{2\pi\rho}{\beta c} = \frac{4\pi}{3}\frac{e^2}{\rho}\beta^3\left[\frac{E}{mc^2}\right]^4. \qquad 3.$$

In practical units (E in GeV, ρ in meters, I in amperes) for a highly relativistic electron ($\beta \approx 1$)

$$\Delta E\,(\text{keV}) = 88.47\, E^4/\rho \qquad 4.$$

Multiplying Equation 4 by the current gives the total radiated power

$$P\,(\text{kW}) = 88.47\, E^4 I/\rho \qquad 5.$$

or in terms of the magnetic field (B in kilogauss)

$$P\,(\text{kW}) = 2.654\, BE^3 I. \qquad 6.$$

Equations 4, 5, and 6 are valid also when the orbit is not circular but consists, as it does in most machines, of arcs of bending radius ρ and field-free straight sections.

Reasonable design parameters for an intermediate energy synchrotron radiation source are $E = 1$ GeV, $B = 10$ kG (corresponding to a bending radius of 3.33 m) and $I = 0.5$ A. Such a machine would radiate 13.3 kW in a continuous spectrum that peaks at about 400 eV and extends to about 3 keV. Larger machines (2–4 GeV) such as SPEAR at Stanford and the National Synchrotron Light Source at Brookhaven National Laboratory (see Tables 1–3) radiate hundreds of kilowatts. At 4 GeV, the photon spectrum of SPEAR extends to about 50 keV. Even larger machines now in construction such as PEP at Stanford and PETRA at Hamburg will reach energies of 15–20 GeV and will radiate several megawatts of synchrotron radiation power with photon spectra extending above 200 keV. Proton storage rings produce negligible synchrotron radiation power because the fourth power dependence on the mass (see Equation 2) reduces the radiated power, compared to electrons, by about 13 orders of magnitude.

The most powerful rotating anode x-ray generators produce only about 10 W of x rays, even though electron beam powers of about 50 kW are used. Almost all of this radiation occurs within a narrow line at the characteristic fluorescence energy of the anode (e.g. 8 keV for copper).

Thus, these sources provide reasonably high intensity at particular photon energies, especially if a large fraction of the isotropically emitted radiation can be used. However, as a continuum x-ray source, synchrotron radiation provides five or more orders of magnitude higher intensity on small experimental samples.

We are assuming that the intensity and spectral distribution of the radiation from N electrons is simply N times that of a single electron i.e. the radiation emission is incoherent between electrons. This is a valid assumption for all cases of interest on present machines. It may be possible for a group of electrons to radiate coherently, producing much higher intensities, if the electron density is high enough and if a density variation with short wavelength components can be produced. This has been analyzed by Csonka (46).

4.2 *Angular and Wavelength Distribution*

For nonrelativistic electrons the angular distribution of the radiation is given by the familiar dipole radiation formula (19)

$$\frac{dP}{d\Omega} = \frac{e^2}{4\pi c^3}\left|\frac{d^2\mathbf{r}}{dt^2}\right|^2 \sin^2\Theta \qquad 7.$$

where Θ is measured relative to the direction of the acceleration. Integration of Equation 7 over all angles yields the Larmor formula, Equation 1. The pattern of the radiation described by Equation 7 is shown in Figure 3, Case I. This would also be the radiation pattern as seen in the instantaneous frame of a relativistic electron.

Light emitted at an angle θ relative to the electron direction of motion in the rest frame is viewed at an angle θ' in the lab frame. The transformation is given by (19)

$$\tan\theta' = \frac{\sin\theta}{\gamma[\beta+\cos\theta]}, \text{ where } \gamma = E/mc^2. \qquad 8.$$

At $\theta = 90°$, $\tan\theta' \approx \theta' \approx \gamma^{-1}$. Thus γ^{-1} is a typical opening half-angle of the radiation in the lab system. The concentration of virtually all of the radiation into such a small forward angle (<1 mrad for machines >1 GeV), as illustrated in Figure 3, Case II, results in extremely high flux densities on small experimental samples even at great distances from the source. For example, at SPEAR a flux of 2×10^{10} photons per second has been measured (47) in a 1-eV bandwidth at 7.1 keV on a 1-mm high by 20-mm wide sample located 24 m from the storage ring operating at 3.7 GeV and 20 mA. In a focusing system a flux of 1×10^{12} photons per second has been measured (47) on a smaller sample but with a 5-eV

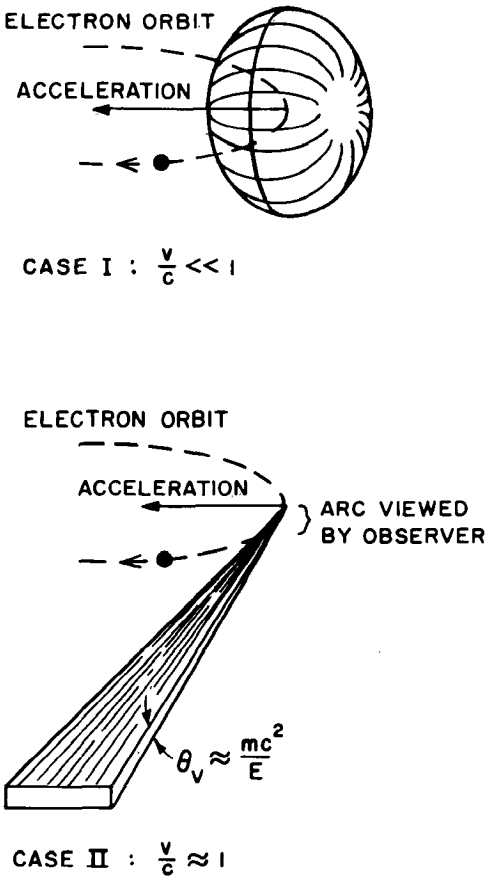

Figure 3 Pattern of radiation emitted by electrons in circular motion. *Case I*: non-relativistic electrons, $v/c \ll 1$. *Case II*: relativistic electrons, $v/c \approx 1$.

bandwidth (other conditions the same) corresponding to a factor of 150 increase in flux density. Even higher fluxes and flux densities will be possible in the future due to dedicated operation of machines like SPEAR at higher currents (39), the use of wigglers, and the operation of new dedicated storage rings designed for high brightness (35).

From Equation 8 it can be shown that the spectrum of the radiation varies as γ^3, as follows: Referring to Figure 4, an observer starts to see a pulse of light when the electron is at position 1 such that the angle, θ, between the electron's direction and the observer's direction is about γ^{-1}. The pulse ends when the electron reaches position 2, where the electron direction is again at an angle γ^{-1} from the observer's direction.

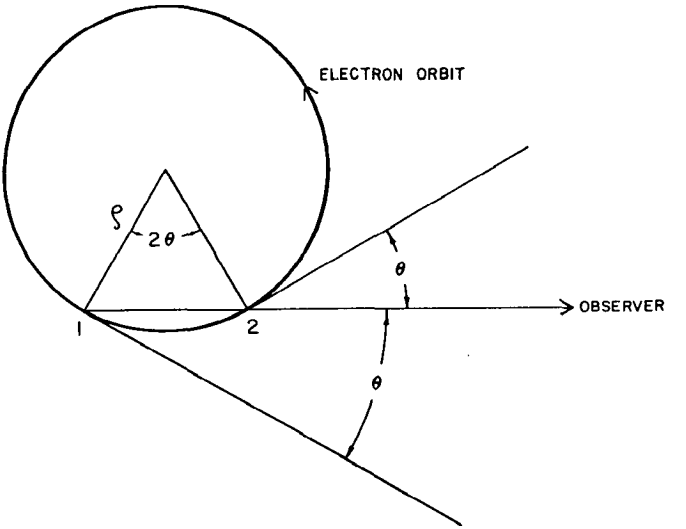

Figure 4 Diagram from which time duration of synchrotron radiation pulse as seen by a stationary observer can be calculated. See text.

For an electron travelling at a velocity β, the duration of the light pulse as seen by the observer is

$$\tau = \frac{\rho}{c}\left[\frac{\theta}{\beta} - 2\sin\left(\frac{\theta}{2}\right)\right] \approx \frac{\rho}{c}\theta^3 = \frac{\rho}{c}\gamma^{-3}.$$

A light pulse of this duration has frequency components up to about $\omega \approx \tau^{-1} = c\gamma^3\rho^{-1}$ corresponding to photon energies of $\varepsilon = \hbar\omega = \hbar c\gamma^3\rho^{-1}$. This can be put into a more convenient form:

$$\varepsilon = \left(\frac{\hbar c}{e^2}\right)\left(\frac{e^2}{mc^2}\right)\gamma^3\frac{mc^2}{\rho} = \frac{r_e}{\alpha}\gamma^3\frac{mc^2}{\rho}, \qquad 9.$$

where

$$\alpha = \frac{e^2}{\hbar c} = \frac{1}{137},\ r_e = \frac{e^2}{mc^2} = 2.8 \times 10^{-15}\ \text{m},\ mc^2 = 0.51\ \text{MeV}.$$

Thus our earlier example of a 1-GeV storage ring with $\rho = 3.33$ m will produce a spectrum that extends to photons with an energy of about 500 eV. This qualitative analysis gives a photon energy, Equation 9, close to the critical energy, defined later in this section (Equation 11), which characterizes the exact spectral distribution. This analysis applies only when the electron is uniformly bent by an angle greater than about

$2\gamma^{-1}$. The interesting case of shorter bending magnets has been analyzed by Coïsson (48).

The results of Schwinger (13), expressed in terms of photon wavelength (26, 42) rather than frequency, give for the instantaneous power radiated per unit wavelength and per radian by a monoenergetic electron in circular orbit

$$I(\lambda\psi) = \frac{27}{32\pi^3}\frac{e^2c}{\rho^3}\left(\frac{\lambda_c}{\lambda}\right)^4 \gamma^8[1+X^2]^2\left[K_{\frac{2}{3}}^2(\xi)+\frac{X^2}{1+X^2}K_{\frac{1}{3}}^2(\xi)\right], \qquad 10.$$

where $X = \gamma\psi$, $\xi = \lambda_c[1+X^2]^{\frac{3}{2}}/2\lambda$, $K_{\frac{1}{3}}$, and $K_{\frac{2}{3}}$ are modified Bessel functions of the second kind, and ψ is the angle between the direction of photon emission and the instantaneous orbital plane (ψ is not the polar angle). The critical wavelength, λ_c, and corresponding critical energy, ε_c are given by

$$\lambda_c = \frac{4\pi\rho}{3\gamma^3}, \quad \varepsilon_c = \frac{3\hbar c\gamma^3}{2\rho}. \qquad 11.$$

[Note: Some authors, including Jackson (19), define the critical wavelength to be twice that given by Equation 11.] In practical units (E in GeV, ρ in meters, B in kG)

$$\lambda_c(\text{Å}) = 5.59\ \rho/E^3 = 186.4/(BE^2)$$
$$\varepsilon_c(\text{keV}) = 2.218\ E^3/\rho = 0.06651\ BE^2. \qquad 12.$$

Half of the total power is radiated above the critical energy and half below. Storage rings and synchrotrons are designed with a fixed value of the bending radius, ρ, in the bending magnets, and hence the bending-magnet field is directly proportional to energy. For technical and economic reasons, the maximum magnetic field is generally chosen to be less than about 12 kG. It is possible to insert special devices (called wigglers) with much higher fields (up to 50 kG for superconducting wigglers) into ring straight sections. This is discussed in the next section.

It is also shown (13, 26, 42) that the angular distribution of radiated power integrated over all wavelengths is

$$I(\psi) = \frac{7}{16}\frac{e^2c}{\rho^2}\gamma^5\left(1+X^2\right)^{-\frac{5}{2}}\left(1+\frac{5}{7}\frac{X^2}{1+X^2}\right), \qquad 13.$$

and integrated over all emission angles the spectral distribution is

$$I(\lambda) = \frac{3^{\frac{5}{2}}}{16\pi^2}\frac{e^2c}{\rho^3}\gamma^7 y^3\int_y^\infty K_{\frac{5}{3}}(\Omega)\,d\Omega, \qquad 14.$$

where $y = \lambda_c/\lambda = \varepsilon/\varepsilon_c$.

The shape of the distribution given by Equation 14 is dependent only on λ_c and is given by

$$G(y) = y^3 \int_y^\infty K_{\frac{5}{3}}(\eta)\, d\eta$$

This function and other related synchrotron radiation functions have been plotted and tabulated (43, 49). Examples of spectral distributions are given in Figure 5.

At the critical wavelength, it may be shown that the total number of photons emitted per second within a 10% bandwidth per milliradian of angle in the orbital plane, integrated over the narrow range of angles out of the orbital plane, is given by

$$N_\gamma = 1.6 \times 10^{15}\, I(\mathrm{A})\, E(\mathrm{GeV}).$$

The photon flux varies slowly for $\lambda > \lambda_c$ but drops exponentially for $\lambda < \lambda_c$. At $\lambda = \frac{1}{5}\lambda_c$ the flux is reduced by a factor of 25 compared to the flux at λ_c. The radiation from a single stored electron is easily detectable (50), including observation of the visible light by eye.

4.3 *Polarization*

The radiation is elliptically polarized with the intensities of the polarization components parallel and perpendicular to the electron orbit given

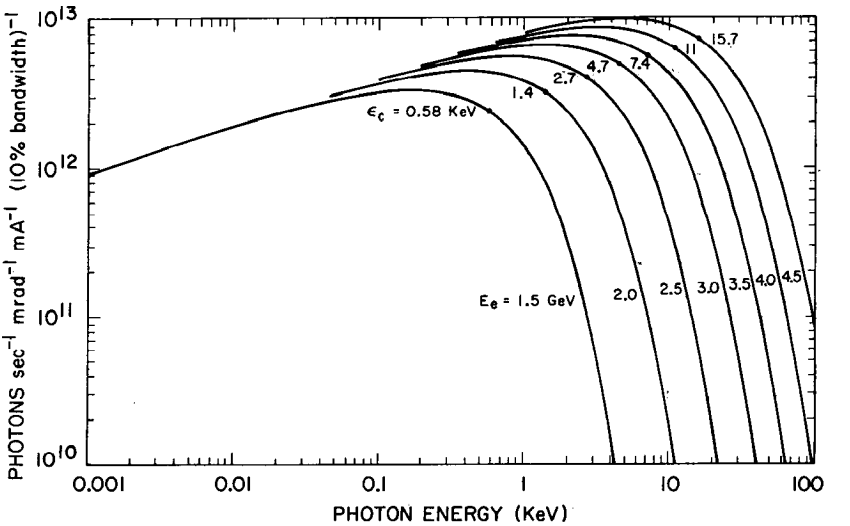

Figure 5 Spectrum of synchrotron radiation from the storage ring SPEAR; bending radius, $\rho = 12.7$ m.

by the two terms of Equation 10. In the plane of the orbit, the radiation is 100% linearly polarized with **E** parallel to the electron acceleration vector. Integration of Equation 10 over all angles and all wavelengths yields a 75% polarization parallel to the orbital plane independent of electron energy and bending radius.

Figure 6 is a plot of the parallel and perpendicular components of polarization as a function of the opening angle for several photon wavelengths. It is clear that polarization can be enhanced by the use of apertures.

Also, in the vacuum ultraviolet (VUV) part of the spectrum, polarization can be enhanced by use of the polarization dependence of reflectance from optical surfaces (51).

Vertically deflecting wiggler magnets (see Section 5) would produce radiation polarized perpendicular to the plane of the ring. Circularly polarized radiation is produced by electrons travelling helical paths as would be produced by special insertions [called helical wigglers (52)] that might be added to storage rings.

4.4 *Pulsed Time Structure*

The radiation is produced in a train of pulses that is different for each ring. The pulse duration, which is determined by the rf system, is typically about 10% of the rf period. The interval between pulses is determined by the pattern of filling of the number of rf wavelengths (or buckets) that can fit into the orbital circumference. For example, SPEAR operates at

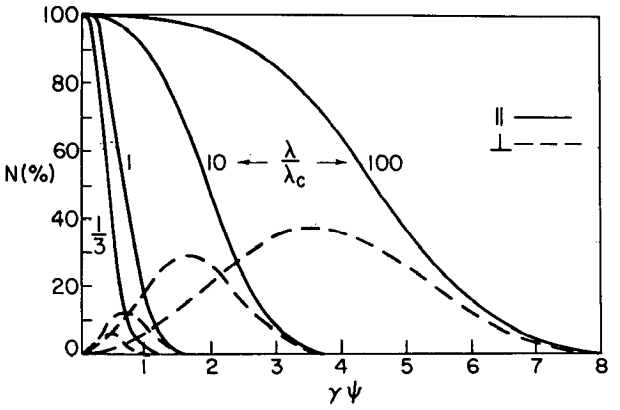

Figure 6 Vertical angular distribution of parallel and perpendicular polarization components. Courtesy of G. K. Green, Brookhaven National Laboratory.

a frequency of 358 MHz, the 280th harmonic of the 1.28 MHz orbital frequency. Thus the pulse length is typically 0.2–0.4 nsec and up to 280 buckets can be filled. By filling one or more desired buckets, a range of pulse intervals from 2.8 to 780 nsec may be obtained. By filling only one bucket, a long interval between pulses is obtained (780 nsec) with greater stability than is possible with multiple buckets each of which may be filled to a different level. This feature is particularly useful in measurements of fluorescence lifetimes.

4.5 *Source Size and Divergence*

As an optical source both the size and angular spread of the electron beam [due largely to betatron oscillations (53, 54)] must be considered. In a storage ring or synchrotron the position of an electron and its angle (both measured relative to the equilibrium orbit) are correlated (53, 54). Phase space plots of radial electron position vs angle in the median plane summarize this correlation in a so-called radial electron emittance ellipse. A similar plot of vertical position vs vertical angle gives the vertical electron emittance ellipse. The precise shape and orientation of these phase space ellipses change from point to point on the electron orbit, but their area (called the electron emittance) is invariant. Low emittance (or high source brightness) is generally desirable. To obtain the actual emittance of the synchrotron radiation the distribution of emission angles of synchrotron radiation must be convoluted with the electron emittances to obtain photon beam emittances.

These can then be used to determine the effect of slits, mirrors, crystals, etc on the spatial distribution and intensity of synchrotron radiation in a real experimental configuration. This use of phase space techniques is discussed further by several authors (43, 55–57).

The actual value of the phase space emittance of electrons is determined largely by the amplitude of the betatron oscillations. The emission of synchrotron radiation is a kind of frictional force that damps these oscillations. However, quantum fluctuations in the emission process excite these oscillations. Thus, the resultant oscillation amplitude and the electron emittance are determined by the balance between the damping and antidamping effects of synchrotron radiation. In a given machine, the electron emittance varies approximately linearly with electron energy. Thus, all machines have their smallest emittance, and therefore highest synchrotron radiation brightness, when operated at their lowest energy. Of course, at lower electron energy the synchrotron radiation spectrum cuts off at lower photon energy, so the above considerations are not the only factor determining the optimum operating conditions of the ring.

5 STANDARD WIGGLERS, INTERFERENCE WIGGLERS, AND THE FREE ELECTRON LASER

Until now, all research with synchrotron radiation has utilized the radiation produced by the ring bending magnets. Plans are now being implemented at several laboratories to utilize special magnetic structures called wigglers, which will enhance and modify the spectrum of synchrotron radiation compared to that produced by the bending magnets. This will considerably extend research possibilities.

The proceedings of a workshop on wiggler magnets (58) gives examples of various designs and analysis of their effects on storage ring performance as well as the properties of wiggler-produced radiation. We briefly summarize the main points here for the two general types of wiggler—the standard wiggler and the interference wiggler or undulator—and the related free electron laser.

5.1 *Standard Wigglers*

A standard wiggler (59–62) consists of several short sections of alternating-polarity transverse field magnets designed to produce no net displacement or deflection of the electron orbit. Thus, such a device could be placed in a field-free region (straight section) of a storage ring or synchrotron. The electron path through such a magnet would resemble a biased sine wave. The magnetic field of the wiggler could be higher (or lower) than that of the ring bending magnets. The synchrotron radiation spectrum would then have a critical energy (see Equation 12) shifted to higher (or lower) photon energy, and there would be an overall flux enhancement due to the superposition of radiation from the several oscillations of the orbit.

For example, an 18-kG wiggler magnet planned (63) for the 1.5-GeV storage ring ADONE would extend the critical energy from 1.5 keV in the bending magnets to 2.5 keV in the wiggler. Superconducting wigglers operating at 35–50 kG would produce even larger increase in critical energy and are being planned at Brookhaven (64), Daresbury (65), and Novosibirsk (G. Kulipanov, private communication). At SSRL, an 18-kG seven-pole wiggler magnet (66) is in construction to extend the synchrotron radiation spectrum when SPEAR operates for colliding-beam experiments with electron beam energies in the 2-GeV region.

Standard wiggler magnets could also be designed to deflect in the vertical plane, which would produce synchrotron radiation with polarization direction perpendicular to that produced by the ring bending magnets. This would be of advantage in certain experimental situations permitting, for example, convenient horizontal reflection by mirrors or crystals without loss of polarization.

5.2 *Interference Wigglers*

A device with many periods designed to produce quasimonochromatic synchrotron radiation is called an interference wiggler or undulator. Several authors have analyzed such devices in helical (52, 67, 68) and transverse geometries (69) or both (70, 71). Other examples of radiation produced by relativistic electrons in periodic fields include the radiation produced by high energy electrons in crystals (72) and Compton backscattering (73). Both of these produce quasimonochromatic peaks and are basically processes similar to interference effects in wigglers.

Interference wigglers can produce peaks in the spectrum of radiation corresponding to wavelengths given by

$$\lambda \approx \frac{\lambda_w}{2\gamma^2}\left[1+\gamma^2\theta^2+\frac{K^2}{2}\right] \qquad 15.$$

where λ_w is the period or repeat length of the magnetic field, $\gamma = E/mc^2$, θ is the angle of observation relative to the average direction of the electron and K is a parameter that depends on the strength and geometry of the wiggler field (52, 70). For example, for a simple sinusoidal field $B_y = B_0 \sin(2\pi z/\lambda_w)$, $K = eB_0\lambda_w/2\pi mc^2 = \psi_0$, where ψ_0 is the maximum angle between the z axis and the approximately sinusoidal trajectory of the electron. The analysis is simplest for the "weak field" case, $K \ll 1$, and then the radiation contains only a single wavelength at each angle θ, given by Equation 15. For $K \gg 1$ (strong fields) larger angular deflections occur, the electron transverse motion becomes relativistic, and harmonics appear (52, 70, 71). The total power radiated at a wavelength given by Equation 15 is maximum for $K = 1$.

The fractional width of the peaks can be no smaller than $1/n$ where n is the number of wiggler oscillations. In a practical case, the width may be further broadened by inhomogeneity in electron energy or magnetic field or particularly if the angular divergence of the electron beam exceeds γ^{-1}. Partly for this reason, new storage ring designs (35) stress low electron beam emittance and provide locations for wiggler insertions where the angular divergence of the electron beam is particularly small.

Recently, measurements have been made on the spectrum and angular distribution produced by an interference wiggler installed in the Pakhra 1.3-GeV synchrotron (74). The ring and magnet parameters were chosen to produce the interference peak in the visible part of the spectrum for convenience.

A practical wiggler for a storage ring might have $\lambda_w \approx 10$ cm. Thus, in a 2-GeV storage ring ($\gamma = 4 \times 10^3$) the interference peak would occur

(Equation 15; $\theta = 0$, $K = 1$) at $\lambda \approx 45$ Å. Peaks at shorter wavelength can be obtained by reducing λ_w or increasing γ. Although some reduction in λ_w could be made, it becomes difficult to design a structure with λ_w less than the transverse aperture requirement for the circulating beam (typically 2–10 cm). Thus, interference peaks in the important region of $\lesssim 1$ Å will require higher energy storage rings such as PEP and PETRA. These machines will have stored beam energy of ≈ 16 GeV ($\gamma \approx 3.2 \times 10^4$) and be capable of producing interference peaks down to 0.7 Å with $\lambda_w = 10$ cm.

Coïsson (75) suggested that an interference wiggler could be used in a high energy ($\gtrsim 200$ GeV) proton machine to produce narrow band synchrotron radiation in the visible part of the spectrum. For example, he calculates (75) that an interference wiggler with a period of 13 cm, a field of 500 gauss, and a length of 5 m would produce more than 10^{11} visible photons per second per milliradian with a 6-A, 400-GeV proton beam. This opens the possibility of monitoring the intensity, cross-sectional area, and energy of such high energy proton beams as is now done on electron machines (76).

5.3 *Free Electron Laser*

This elegant and intriguing device is basically an interference wiggler structure (as described in the preceding section) plus a pair of mirrors forming a resonant cavity. Under the correct conditions, the mirrors provide feedback resulting in stimulated emission at a wavelength given by Equation 15. The device was first suggested by Madey (77), whose group was the first to demonstrate gain (78) and lasing action (79) in the device, using a linear accelerator as a source of electrons in both experiments. Several other authors have analyzed the device (80).

Although important in verifying the theory and establishing the practicality of the device, the experiments of Madey and co-workers (78, 79) produced only small average laser power (0.36 W, although the peak power was 7 kW) and at low efficiency (the total energy collected on the detector was 0.01% of the electron beam energy). By incorporating the device into an electron storage ring as shown schematically in Figure 7, much higher power at high efficiency may be attainable, thus providing the basis of a new class of tunable lasers.

A variation of the free electron laser, called the optical klystron, has been suggested by Vinokurov & Skrinskii (81). Their analysis shows that the threshold current for lasing can be reduced (perhaps by a factor of 10^3) in their two-stage device.

Neither the free electron laser nor the optical klystron has yet been tried in an electron storage ring. Studies for specially designed small

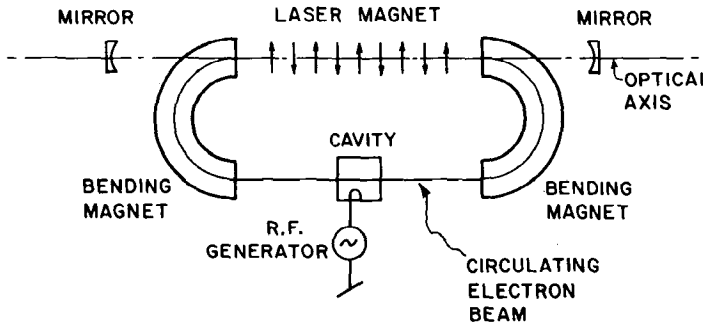

Figure 7 Schematic of free electron laser incorporated into an electron storage ring. Courtesy of J. M. J. Madey, Stanford University.

storage rings to incorporate such devices are in progress (private communications from C. Pellegrini and J. M. J. Madey).

6 INSTRUMENTATION FOR THE UTILIZATION OF SYNCHROTRON RADIATION

Much specialized instrumentation is required to collect, transport, monochromatize, and focus the synchrotron radiation onto an experimental sample and then to detect the transmitted, diffracted, or scattered photons or secondary electrons produced. It is clear that the development of instrumentation optimized for the characteristics of synchrotron radiation has already significantly expanded the research capabilities. Much remains to be done in this area, because many of the instruments now used were developed for other radiation sources and are not optimized for synchrotron radiation research. For example, advances are being made in the fabrication and polishing of mirrors (82) to reflect and focus synchrotron radiation in the VUV and x-ray regions using grazing incidence and total external reflection. Also multilayer reflective coatings (83) are being developed for normal incidence use in the VUV region.

Here, we give only a few examples of synchrotron radiation research instrumentation. More information can be found in the proceedings of several conferences and workshops on the subject (84–86) and in detailed descriptions of particular laboratories (2–5).

6.1 *Monochromators*

Perhaps the most important single instrument for research with synchrotron radiation is the monochromator. Specialized monochromators

for the vacuum ultraviolet, soft x-ray, and hard x-ray regions of the spectrum are described in the above-mentioned proceedings and laboratory descriptions. A particularly successful vacuum ultraviolet and soft x-ray grazing incidence grating monochromator called the "Grasshopper" has been designed by Brown, Bachrach & Lien (87) and utilized since 1974 at SSRL. It covers an unusually large energy range (32 eV to $\gtrsim$1500 eV). At DESY, Eberhardt and co-workers (88) have designed and built a grating monochromator called "Flipper," which covers a narrower energy range (20–300 eV) but with excellent order-sorting capabilities. More recently, instruments based on holographically made toroidal reflection gratings (89) appear to offer extremely high efficiency up to about 150 eV. Several authors (90, 91) suggest that holographically made transmission gratings can open up new possibilities for vacuum ultraviolet and soft x-ray monochromators. A review of monochromator designs for the VUV spectral region is given by Pruett (92). Sagawa (93) reviewed monochromators developed for synchrotron radiation use in Japan.

In the harder x-ray region, Bragg diffraction from crystals (e.g. Si, Ge, graphite) is the basis of monochromator designs. A review of the many possible configurations was given by Hastings (94) as well as by Beaumont & Hart (95). A very versatile yet simple monochromator utilizes a plane channel-cut crystal. Such a device was very successfully implemented by Kincaid (96) at SSRL in 1974 and is used extensively in many experiments, particularly on studies of Extended X-Ray Absorption Fine Structure (EXAFS) as described in Section 7 of this review. It provides rapid tunability, high transmission, narrow bandwidth ($\Delta E/E \approx 10^{-4}$), and almost constant exit beam position and direction.

In 1976, a major increase in capability was achieved with the implementation of a focusing version of this device by Hastings, Kincaid & Eisenberger (47) at SSRL. This powerful monochromator system employs a toroidal double-focusing mirror [first used by Horowitz (97)] in conjunction with a two-crystal monochromator. The properties of double-focusing grazing incidence mirrors were studied by Howell & Horowitz (98). The ability to adjust the crystals relative to one another facilitates compensation for thermal effects on the first crystal due to high power densities of focused radiation, and permits the suppression of harmonics. The mirror collects a large amount of synchrotron radiation and focuses it into a small spot (2 mm × 4 mm) resulting in flux densities 150 times higher than in unfocused beams. The platinum coated mirror is used at a grazing angle of incidence of 10 mrad, which reflects x rays up to $\sim$9 keV with high efficiency but cuts off sharply at higher energy. This provides excellent rejection of harmonics above $\sim$10 keV. The system is shown in Figure 8.

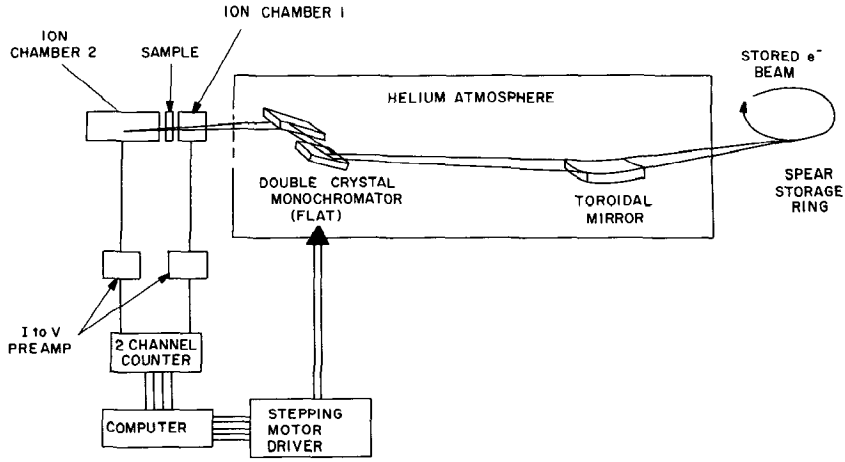

Figure 8 Schematic of separated function monochromator system. See discussion in text. Courtesy of J. Hastings, Brookhaven National Laboratory.

6.2 *Detectors*

A large variety of detectors have been used in synchrotron radiation research including scintillation counters, position sensitive detectors, photographic film, proportional counters, channeltrons, image intensifier systems, solid state detectors, and ionization chambers. A review of x-ray detectors for synchrotron radiation was given by Brown (99). Reviews of electronic area detectors of several types are given in chapters of a recently published book (100).

Improvements in many of the detectors have been made to meet the requirements of synchrotron radiation research (e.g. high counting rate, better angular and energy resolution). There is a particularly important need for the development of area detectors with good spatial resolution and high counting-rate capability to replace film as a recording medium, for example, in recording x-ray diffraction patterns. Developmental programs for such detectors are under way in several synchrotron radiation research laboratories (DESY, Novosibirsk, Orsay, SSRL).

A multiwire proportional chamber (MWPC) system has been developed by Xuong and co-workers (101) using a chamber developed by Perez-Mendez. The system has been used to solve protein structures by recording diffraction patterns generated by a conventional x-ray tube. A very promising MWPC system capable of higher counting rates and improved spatial resolution is the spherical drift chamber as developed by Charpak and co-workers (102). Several reports on position sensitive detectors were

presented at the Orsay Instrumentation Conference (85) and at the Stanford Workshop on X-Ray Instrumentation for Synchrotron Radiation Research (86).

7 APPLICATIONS OF SYNCHROTRON RADIATION

In this main section of our review, we discuss several applications of synchrotron radiation to basic and applied research and technology. From the very large amount of work that has been done, we have tried to select important recent developments and those that best illustrate the special characteristics and capabilities of synchrotron radiation. We also include several suggested applications, some speculative, that may be developed in the future.

We have found it impossible, however, to be complete. The spectrum of scientific and technological activities affected by synchrotron radiation is so broad in scope that it is beyond our capabilities to describe all of them well. These activities range from determination of biological structures to analyses of electronic structures of metals and semiconductors at surfaces, using techniques that vary from the scattering and absorption of x rays to photoemission induced by ultraviolet radiation. Since one of us is close to the x-ray absorption and diffraction fields, and since synchrotron radiation activities in these fields are new and not yet described by such a review, we have concentrated more on these and less on the equally important, but more completely, previously described research lines in the ultraviolet portion of the spectrum.

Of necessity, several applications are not covered at all. These include: (*a*) the use of synchrotron radiation as a radiometric standard (42, 103); (*b*) the calibration and characterization of instrumentation such as gratings (104) and detectors; (*c*) the use of synchrotron radiation as a monitor and diagnostic tool in electron synchrotrons and storage rings (76) to measure the intensity, bunch dimensions, and energy of circulating electron beams; (*d*) radiation damage studies including the simulation of plasma conditions (105); (*e*) synchrotron radiation as an infrared source (106).

7.1 *X-Ray Diffraction*

7.1.1 INTRODUCTION X-ray diffraction has been, for over fifty years, the basic tool for the determination of atomic arrangements in condensed matter. Synchrotron radiation offers the potential for major improvements in a number of experimental approaches because of its unique characteristics. In particular, as discussed in separate sections below, the

capability of choosing the wavelength to be employed in an experiment, rather than being restricted to the characteristic radiations produced by x-ray tube anode materials, makes possible the exploitation of anomalous scattering in structure determinations. The intense white radiation makes possible experiments in which x-ray diffraction intensities can be measured extremely rapidly by sorting photon energy electronically (i.e. pulse height analysis) rather than by mechanical angular scans. In addition, it allows for the rapid production of x-ray topographs. Finally, the high degree of natural collimation of the beam leads to relatively simple small-angle scattering experiments as well as high resolution x-ray topographs. These applications are discussed in the sections that follow. Before proceeding, however, we review briefly some of the basics of x-ray diffraction.

The geometry of a typical experiment is shown in Figure 9. There, $\mathbf{k}_0$ and $\mathbf{k}'$ (of magnitude $2\pi/\lambda$ where λ is the x-ray wavelength) are the wave vectors of the incident and diffracted beams, respectively. It is convenient to describe the scattering process in terms of the diffraction vector, which is defined by the relationship

$$\mathbf{k} = \mathbf{k}' - \mathbf{k}_0. \tag{16.}$$

It is easily shown that

$$|\mathbf{k}| = 4\pi \sin \theta/\lambda. \tag{17.}$$

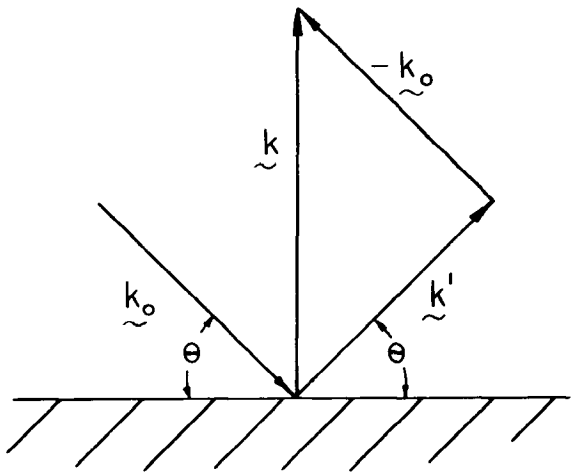

Figure 9 Geometry of Bragg scattering. $\mathbf{k}_0$ and $\mathbf{k}'$ are the wave vectors of the incident and diffracted beams, respectively.

In most diffraction experiments, the incident photon energies are far from the absorption edge energies of the atoms in the sample and, in addition, multiple scattering of the x rays can be neglected. In this case, the diffracted intensities, $I(\mathbf{k})$, are related to the electron density, $\rho(\mathbf{r})$, in the sample through the following relationships.

$$I(\mathbf{k}) = C(\mathbf{k}) \left| F(\mathbf{k}) \right|^2, \tag{18.}$$

where

$$F(\mathbf{k}) = \int \rho(\mathbf{r}) \exp(i\mathbf{k} \cdot \mathbf{r})\, d\mathbf{r} \tag{19.}$$

and $C(\mathbf{k})$ is a slowly varying function of $\mathbf{k}$ that depends on the geometry of the experiment. Thus, the scattering amplitude, $F(\mathbf{k})$, is the Fourier transform of the electron density. To further simplify, we define the atomic scattering factor f_i^0 of the ith atom through the relation

$$f_i^0(\mathbf{k}) = \int \rho_i(\mathbf{r}) \exp(i\mathbf{k} \cdot \mathbf{r})\, d\mathbf{r}, \tag{20.}$$

where $\rho_i(\mathbf{r})$ is the electron density associated with the ith atom, but with $\mathbf{r}$ now measured relative to the center of that atom. Then, Equation 19 can be rewritten in its common form as the structure factor

$$F(\mathbf{k}) = \Sigma_i f_i^0 \exp(i\mathbf{k} \cdot \mathbf{r}_i), \tag{21.}$$

where the summation is over all the atoms in the sample. In a crystalline material, this may be expressed as N times the summation over one unit cell for Bragg reflections. Here, N is the number of unit cells. A unit cell is the basic repeating element in the crystal.

Equation 19 implies that if $F(\mathbf{k})$ were a measurable quantity, its Fourier transform would yield the electron density, which would be the maximum information obtainable about the atomic arrangement. Unfortunately, only the magnitude of $F(\mathbf{k})$ can, in general, be obtained through diffraction experiments. The phase associated with this complex quantity cannot be determined directly. This indeterminability leads to difficulties and ambiguities in determining crystal structures from x-ray diffraction data. For example, in protein crystal structure determinations, it is common to obtain these phases through the method of multiple isomorphous substitution. In this method, diffraction data are gathered from a number of similar crystals, which differ chemically only in that each crystal has a different heavy atom substituted into a specific known atomic site. It is assumed that the basic structure of the protein is undisturbed by this substitution. The differences in intensities are used to

determine the phases. The method works only when suitable isomorphous derivatives can be prepared, a limited subset of all protein crystals. The anomalous scattering of x-rays offers a different approach, as explained below.

7.1.2 ANOMALOUS SCATTERING When the incident photon energy is close to that of an absorption edge of an atom in the sample, Equations 19 and 20 are no longer valid. Instead, the atomic scattering factor, as used in Equation 21 must be replaced by

$$f_i = f_i^0 + \Delta f_i' + i\Delta f_i''. \qquad 22.$$

Here, i, $\Delta f_i'$, and $\Delta f_i''$ are real functions of both photon energy and scattering vector magnitude, k. This phenomenon is reviewed by James (107) and by Ramaseshan & Abrahams (108). The forms of $\Delta f'$ and $\Delta f''$ near an absorption edge are shown in Figure 10. It is important to note that $\Delta f'$ becomes large and negative for photon energies just below the edge energy, so that large changes in f_i can be achieved through variation

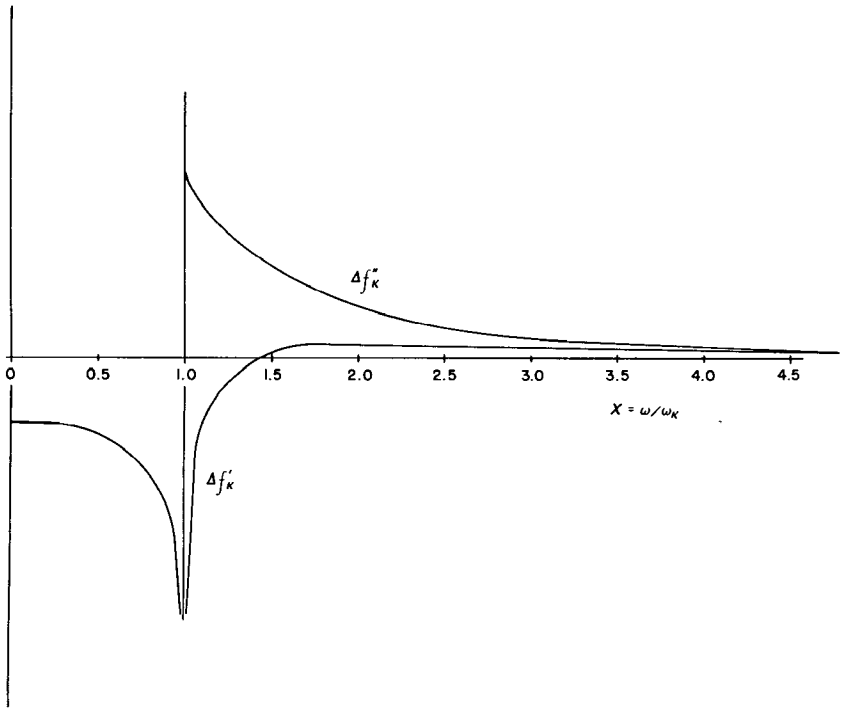

Figure 10 Real, f', and imaginary, f'', shifts of the atomic scattering factor as a function of angular frequency, ω, near an absorption edge, ω_K.

of the x-ray wavelength near the absorption edge. These changes have been employed by Phillips et al (109) in their synchrotron radiation study of the protein rubredoxin. This paper contains the details of the analysis as well as a large bibliography dealing with the theory of the use of anomalous scattering for this purpose. The great advantage of synchrotron radiation for this purpose is that λ can be tuned to achieve maximum changes in the f_i. It should also be noted, however, that Phillips et al (110) have also shown that the diffracted intensities observed in their synchrotron radiation experiments are a factor of at least 60 greater than those obtained with a sealed x-ray tube using the same crystal and instrumental parameters. In addition, in the few protein crystals studied with synchrotron radiation, it appears that there is essentially no loss of diffracting power during an exposure lasting several minutes. With conventional sources, exposures are often many hours, and radiation damage often causes reduced diffraction capability toward the end of the exposure. It appears that there are some radiation damage effects with a time constant measured in hours or days, since the crystals exposed to synchrotron radiation are badly damaged and diffract poorly several days later, even though they did not degrade measurably during the brief exposure. This is extremely important, since degradation of the protein crystals in the x-ray beam, coupled with the long exposure time and difficulties of producing crystalline samples, are major limitations in performing protein crystal structure analysis with conventional x-ray tubes.

Anomalous scattering has also been employed in the study of binary alloy order-disorder critical phenomena. In such phenomena, the alloy of composition AB is arranged in an ordered fashion at low temperatures. In CuZn, for example, the Cu atoms can be assigned to the corners of a cubic unit cell, while the Zn atoms occupy the body centers. As the temperature is elevated, the Cu and Zn atoms interchange positions until, at the critical temperature of approximately 460°C, the Cu and Zn atoms are equally distributed over the two sites.

The diffraction patterns from such alloys consist of two types of Bragg reflections plus a diffuse scattering, as discussed extensively by Guttman (111). One type of Bragg scattering comes from reflections whose intensities are independent of the state of order. These intensities are proportional to $|f_A+f_B|^2$. Those reflections that provide information about the state of long-range order in the material (i.e. the occupancies of the two different sites) have intensities proportional to $|f_A-f_B|^2$. Similarly, the diffuse scattering, which is related to the short-range order, or the probability that each A is surrounded by B atoms, is proportional to $|f_A-f_B|^2$.

It is usually difficult to measure the scattering that depends on the $|f_A - f_B|^2$, the order dependent scattering, because the alloys that show such transitions, (e.g. CuZn and CoFe) contain elements adjacent on the periodic table. As a result, there is little difference in their atomic scattering factors. The difference can be magnified greatly by tuning the photon energy to just below the absorption edge energy of either the A or B atom, so that the anomalous scattering is large. Synchrotron radiation experiments employing this approach have been performed by Sparks (unpublished).

It has also been proposed to use anomalous scattering of x rays to aid in the determination of atomic arrangements in amorphous materials. One approach, proposed by Keating (112) and discussed extensively by Bienenstock (113), involves the measurement of intensities diffracted by an amorphous binary (A-B) material at three different wavelengths. With such measurements, it should be possible to obtain separate A-A, A-B, and B-B atomic pair correlation functions. This method has been attempted using standard x-ray tubes by Waseda & Tamaki (114). Under such circumstances, when one cannot tune close to the edge, the method is extremely sensitive to experimental error, as discussed by Fuoss & Bienenstock (115). Since, however, the reliability of this approach can be increased markedly with increasing differences in the atomic scattering factors associated with the three different x-ray wavelengths, synchrotron radiation tunability offers the potential for further development of this technique as a reliable structural tool. However, a complete set of experiments has not yet been performed, although it has been initiated by Fuoss and co-workers.

The second approach, proposed by Shevchik (116), uses the strong variation with wavelength of the anomalous scattering factors near the absorption edge to obtain the coordination of individual atomic species in polyatomic amorphous materials. Because this variation is strong near the edge and weak everywhere else, the first and second derivatives of the intensity with respect to wavelength are determined by the coordination of the atomic species associated with the edge. Again, it is the tunability of the synchrotron radiation that makes this experiment feasible, although it has not, to our knowledge, been performed yet.

As discussed in Section 7.1.3, anomalous scattering may also be employed in small-angle x-ray scattering to increase the contrast between two phases.

The availability of tunable x-ray sources and the increased interest in the employment of anomalous dispersion has also lead to utilization of synchrotron radiation for the determination of $\Delta f'$ and $\Delta f''$. Such measurements are quite important because the methods described above

depend rather sensitively on accurate knowledge of the wavelength dependence of these parameters. Bonse & Materlik (117) used an x-ray interferometric technique (118) to measure $\Delta f'$ for Ni. Fukamachi et al (119) studied the wavelength dependence of the relative intensities of centrosymmetric pairs of reflections to obtain $\Delta f''$ for Ga in GaP. Finally, Hodgson, Templeton, and co-workers (private communication) recently observed a $\Delta f''$ of over 20 for Cs, very close to its absorption edge. This important result implies that utilization of anomalous dispersion will increase markedly in the near future.

7.1.3 SMALL-ANGLE X-RAY SCATTERING Small-angle x-ray scattering is the measurement of the scattering of x rays for small values of k. From Equations 17 and 19 it is apparent that such scattering is sensitive to long wavelength components of the electron density fluctuations. Consequently, it is commonly employed to obtain information about the size and shape of large (e.g. protein) molecules, the form of phase separation in a multicomponent alloy, or the form of the density fluctuations associated with critical phenomena.

Synchrotron radiation offers three advantages over x-ray tubes for the performance of this work. The first, and most important, is the natural collimation of the beam, which eliminates the necessity for the normally required sophisticated collimation systems to separate the diffracted from the transmitted beam. This natural collimation also leads to an extremely high usable intensity, relative to a normal x-ray tube. Finally, synchrotron radiation offers the possibility of obtaining increased contrast in special circumstances where a sample consists of two or more phases with almost the same electron density, but different chemical compositions. According to Equation 19, the intensity of normal scattering is rather small under such circumstances. By tuning the radiation close to the absorption edge of an element present in one phase, however, the effective contrast in electron density and the corresponding intensity can be made quite large.

A most dramatic display of the first two of these advantages is work carried out at Novosibirsk on the VEPP-3 storage ring as reported by Kulipanov & Skrinskii (50). The small-angle diffraction from frog muscle was recorded by means of a one-dimensional position-sensitive detector and accompanying multichannel analysis. Contraction of the muscle was produced by electrical excitation with a special stimulator triggered by pulses from a synchronizing generator. This generator synchronized the operation of the detecting apparatus with the phase of the muscle contraction. The muscle contraction cycle ($\sim$64 msec) was broken down into eight time intervals, and information from the detector in each of the

intervals was recorded in one of the eight groups of the analyzer memory. This detection system permitted an eight-frame film to be made and permitted the change in the muscle structure to be observed in the various phases of the contraction. The first experiment was carried out by superposition of the information obtained from 100 muscle contractions. By contrast, many hours are required for the observation of usable small-angle diffraction data from muscle with a standard x-ray tube, and dynamic experiments are therefore difficult or impossible. With the increased intensity expected from synchrotron radiation sources in the future, it should be possible to obtain a complete diffraction pattern in a few milliseconds, and therefore a series of diffraction patterns could be recorded during a single muscle contraction.

Extensive studies, both static and dynamic, performed at DESY on muscle or muscle-related material have been described in the review of applications of synchrotron radiation to biological structure and chemical analysis by Barrington Leigh & Rosenbaum (120). Bordas et al (121) have reported work on rat tendon using the energy dispersive detector technique described below, while Kretzschmar et al (submitted for publication) have reported a detailed analysis of the shape and size of myosin subfragment-1. Blaurock (122) has shown that stacking disorder is characteristic of myelin in a freshly dissected nerve, using the small-angle mirror-monochromator system described by Webb (123).

7.1.4 ENERGY DISPERSIVE DETECTORS FOR POWDER DIFFRACTOMETRY AND SMALL-ANGLE SCATTERING In most x-ray diffraction experiments employing a standard x-ray tube, it is customary to scan **k**-space by varying the scattering angle and using monochromatic radiation (see Equation 17). Such an approach takes advantage of the very large ratio of characteristic to white radiation intensities produced by an x-ray tube.

An alternative approach, employing the white synchrotron radiation and energy dispersive detectors, has been explored recently. In this approach, the detector is held at fixed scattering angle and has incident upon it radiation of all wavelengths scattered by the sample. The lithium-drifted silicon or germanium detector then sends to a multichannel analyzer a signal that is dependent on the x-ray photon energy. Thus **k**-space is covered by sorting diffracted photon energies by electronic means. The method has been used for powder diffractometry by Buras et al (124) and by Bordas et al (125). Small-angle scattering experiments on biological materials have also been performed by Bordas et al (121) in this manner.

The major advantage of this technique is the speed of data acquisition; diffraction patterns are obtained in a few seconds under optimum

conditions. This speed should make possible the diffraction analysis of dynamic phenomena like phase transitions and biological changes.

7.1.5 TOPOGRAPHY X-ray topography has been used for many years as a technique for imaging defects, cracks, voids, dislocations, etc in crystals. In this technique, the intensity of Bragg reflection as a function of position on the reflecting planes is measured carefully, yielding an image of that plane. Contrast is achieved in the image because of the difference in reflecting power between the perfect and distorted parts of the crystals.

Synchrotron radiation appears to be an ideal source for x-ray topography for the following reasons:

1. The high intensity reduces exposure times by two to four orders of magnitude.
2. The entire white spectrum can be used, or a narrow band can be selected with a monochromator. The use of white radiation offers two very great advantages. The first is that extremely simple crystal mounting techniques can be used since each Bragg reflection picks out the appropriate wavelength for diffraction. As a result, the topography measurements can be performed readily in combination with magnetic field or temperature variations. In addition, the high intensity means that very short exposures are required, so dynamic effects can be studied.
3. The extremely small angular divergence ($\sim 10^{-4}$ rad for multi-GeV machines) permits high spatial resolution ($\sim$microns).

The general features of white radiation topography were explored by several groups including Tuomi et al (126) using the DESY synchrotron, Hart (127) using the Daresbury synchrotron, and more recently Parrish & Erickson (unpublished) using the SPEAR storage ring. The simple geometry used in these experiments is shown in Figure 11. Figure 12 gives some results. There have been many time dependent experiments,

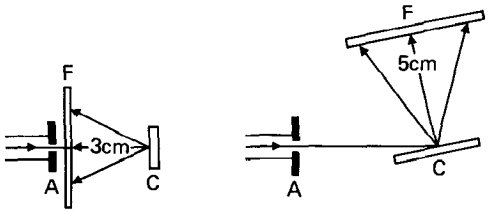

Figure 11 Geometry for x-ray topography with broadband synchrotron radiation (A = Aperture, F = Film, C = Crystal). (*Left*) Arrangement for back reflection. (*Right*) Arrangement for grazing incidence. Courtesy of W. Parrish, IBM, San Jose, CA.

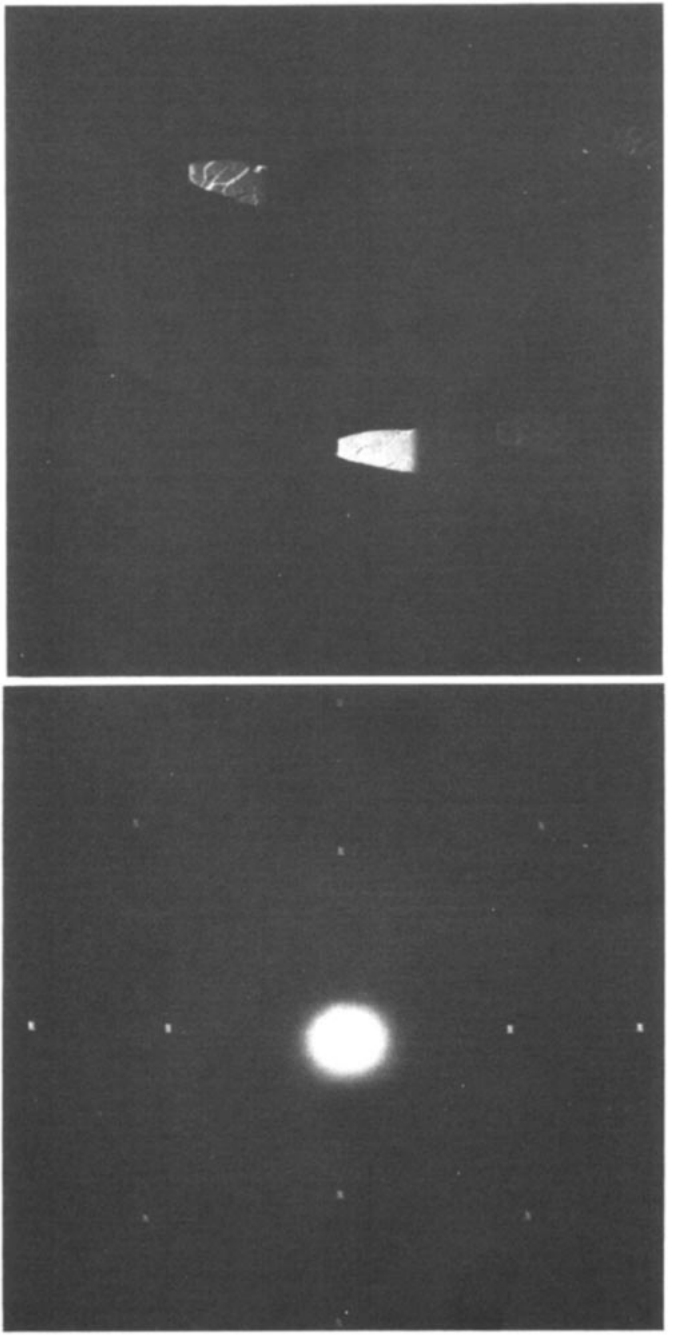

Figure 12 X-ray topographs of lithium fluoride cleavage surface. (*Bottom left*) Back reflection on Polaroid film 3 cm from sample. Exposure is 3 min with SPEAR at 1.85 GeV, 6.8 mA. (*Bottom right*) Grazing incidence on Kodak R single-coated film 5 cm from sample. Exposure is 5 min with SPEAR at 1.89 GeV, 7.2 mA. (*Top*) Optical enlargement of upper reflection spot in bottom right figure. Courtesy of W. Parrish, IBM, San Jose, CA.

including the study of phase transitions (128), domain wall motion (129), plastic deformation (130), and recrystallization (130). Composite crystals have been studied by several groups using synchrotron radiation including studies of polytypes in ZnS (131), bicrystals in germanium, and various heteroepitaxial systems (132).

It is clear that x-ray topography with synchrotron radiation will continue to attract more workers particularly on the large storage rings such as DORIS, DCI, SPEAR, and VEPP-3 that are ideally suited for these studies.

7.1.6 COHERENT NUCLEAR SCATTERING—MÖSSBAUER EFFECT The high brightness, high polarization, and pulsed time structure of synchrotron radiation open the possibility of performing experiments on coherent nuclear scattering with improved intensities (compared to radioactive sources) and at any desired photon energy. Certain (Mössbauer) nuclei have, at an extremely well-defined energy, scattering amplitudes exceeding that of all their electrons. If crystals made only of such nuclei were available, it would be possible to Bragg-reflect photons of only that energy from the incident beam. For example, with ^{57}Fe, a 14-keV x-ray beam with energy defined to one part in 10^{11} can be obtained. This is five or six orders of magnitude better than can presently be achieved with conventional crystal monochromators. With present synchrotron sources such as SPEAR more than 10^4 photons per second are available within this narrow energy range. With dedicated operation and with wigglers, two or more orders of magnitude could be gained.

The primary experimental problem is to observe the narrow band radiation from the decay of the nuclear resonantly scattered radiation (lifetime $\sim$ 100 nsec) in the presence of an intense, brief ($\sim$0.3 nsec) prompt pulse. This can be accomplished in several ways including the following:

1. Suppression of the wider band ($\sim$1 eV) atomic electronic Bragg-scattered radiation may be obtained using the fact that this radiation is electric dipole whereas the resonant nuclear scattering is magnetic dipole, i.e. the polarization selection rules differ.
2. The much larger nuclear cross section makes it possible to use very thin crystals, which are nearly transparent to electronic processes.
3. By using a multicomponent crystal, the electronic scattering from different types of atoms can be made to cancel approximately.
4. The larger Darwin width for nuclear reflections makes it possible to use successive reflections from two slightly misoriented crystals such that overlap of the nuclear scattering is large and that of the electronic scattering is small.

Efforts are under way by groups in Novosibirsk (V. A. Kabannik, private communication) and Stanford (P. A. Flinn, S. L. Ruby, private communication; and R. L. Cohen, G. L. Miller, private communication) to solve the technical problems involved such as obtaining sufficiently perfect, isotopically enriched single crystals containing ^{57}Fe and developing special gated detectors to register delayed emission of photons or conversion electrons.

If these efforts are successful, they will facilitate study of coherent nuclear scattering and open exciting possibilities in x-ray interferometry and holography, for which the large coherence length (~ 1 m) of these photons is a vital new property. Full exploitation of the potential of this highly monochromatic radiation (for x-ray holography, for example) will require the higher intensity that should be available in the future and also the development of higher resolution recording media. Meanwhile, it should be possible, for example, to duplicate the classical interference experiments, such as the Fresnel biprism, in the x-ray region.

More detailed treatments of coherent nuclear scattering with synchrotron radiation are given in the literature (50, 133, 134).

7.2 *Extended X-Ray Absorption Fine Structure*

7.2.1 INTRODUCTION The development of Extended X-Ray Absorption Fine Structure (EXAFS) analysis as a means of determining the local coordination environment of individual atomic species in complex, polyatomic materials is one of the most important results of the availability of synchrotron radiation in the x-ray regime. Unlike the single-crystal diffraction techniques, this method may be applied to the determination of such coordinations for: (*a*) noncrystalline and poorly crystallized materials, as well as crystalline materials; and (*b*) dilute impurities in crystalline or amorphous materials. Here, by coordination we mean the number and type of atoms surrounding a specific atom and the interatomic distances.

These types of structural problems are often of considerable scientific and/or technological interest, since the determination of atomic arrangements is usually the first step in obtaining microscopic understanding of the physical and chemical properties of condensed matter. For example, the importance of these classes of problems becomes clear when one notes that most glasses used commercially or scientifically contain mixtures of SiO_2 or B_2O_3 with a number of metal oxides, which are added to control physical properties. Little is known about the coordination of the metal atoms. Similarly, small concentrations of impurities are used to control the electrical properties of crystalline and

amorphous semiconductors. Their electrical action is intimately linked to their coordination. Finally, it is believed that the biological action of many large molecules is mediated by changes in the coordination geometry of metal atoms, which are often present in low concentrations.

While some techniques, such as nuclear magnetic resonance or electron spin resonance, might be applied to specific atomic species for the determination of coordination, there was no generally applicable approach prior to the development of EXAFS analysis.

The EXAFS is the fine structure on the x-ray absorption coefficient that appears for photon energies in the range of approximately 0–1500 eV above an absorption edge, as illustrated in Figure 13. Here, Hunter's (135) measurements of the relative absorption coefficient of crystalline $CuAsSe_2$ are shown as a function of photon energy in the region of the Cu K edge near 9 keV. For photon energies below the edge, the absorption coefficient, which is due here to lower energy processes, is a slowly varying and monotonically decreasing function of photon energy. At the edge, the photon has enough energy to excite the K-shell electron to the lowest energy empty states, yielding the sharp increase in the absorption coefficient. This change is shown more clearly in Figure 14, in which the absorption due to the lower energy processes has been subtracted out. Above the edge, the absorption coefficient consists of a slowly varying, monotonically decreasing part, superimposed upon which is a fine structure, the EXAFS.

As is discussed extensively below, this fine structure results from the backscattering of the photoelectron by the atoms surrounding that from which the electron was ejected. Consequently, it may be analyzed to obtain information about the average coordination of the atomic species

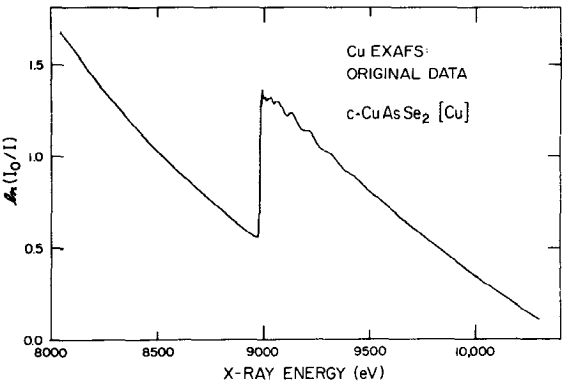

Figure 13 Relative x-ray absorption coefficient of crystalline $CuAsSe_2$ as a function of x-ray energy near the Cu absorption edge. Courtesy of S. Hunter, SSRL.

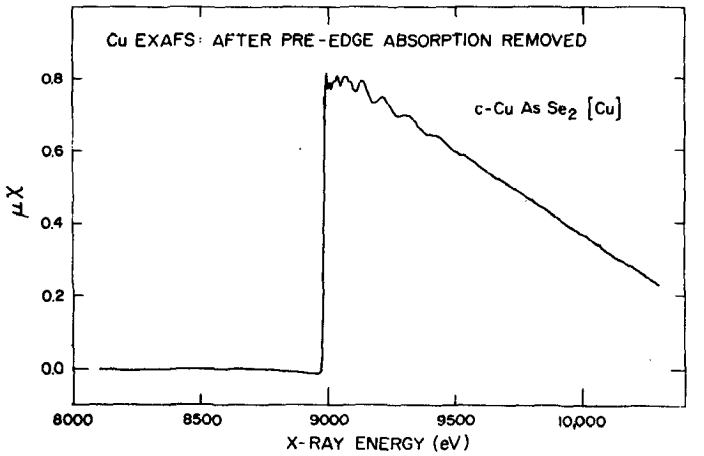

Figure 14 Relative x-ray absorption coefficient of crystalline $CuAsSe_2$ after removal of pre-edge absorption, as a function of x-ray energy near the Cu absorption edge. Courtesy of S. Hunter, SSRL.

whose absorption edge is being studied. Thus, if the absorption edges of all the atomic species in a sample being studied are sufficiently separated in energy, the average coordination of each may be determined separately through studies of the EXAFS associated with each edge. This feature makes EXAFS analysis a powerful structural tool in problems of the type discussed in this section.

Although EXAFS has been observed for nearly half a century, its importance as a structural tool became apparent through the pioneering work of Lytle (136, 137) and then Sayers et al (138, 139) in the mid-1960s and early 1970s. The availability of synchrotron radiation in the x-ray region during the past few years has led to dramatic progress in EXAFS data acquisition and analysis.

From the experimental point of view, the progress has been vastly accelerated because synchrotron radiation provides high intensity over a broad spectral range and is thus well suited for studies of the absorption coefficient as a function of photon energy over an extended energy range. In contrast, the classical x-ray tube source provides a high intensity of characteristic radiation at specific photon energies, but a very low intensity of the continuous Bremsstrahlung needed for such studies. As a result, a very large part of all the experimental EXAFS work published thus far has been performed at the Stanford Synchrotron Radiation Laboratory. It should also be noted that the polarization of synchrotron radiation makes it naturally useful for EXAFS studies of anisotropic

materials. For such studies, radiation from a tube source must be polarized in a separate step, which further decreases the available intensity.

7.2.2 EXAFS—SOME BASIC CONSIDERATIONS In order to provide a basis for the review of recent EXAFS research, the fundamental theory of Sayers et al (139) as well as of Ashley & Doniach (140) is reviewed here. As indicated above, the x-ray absorption process consists of the ejection of an electron from an atomic core state by a photon of energy E. Since the resulting photoelectron's energy is large relative to binding energies in the material, it may be considered as almost free, so that its wave-number magnitude, k, may be well defined by the relation

$$\hbar^2k^2/2m = E - E_0, \qquad 23.$$

where E and E_0 are the photon and the absorption edge energies, respectively. The EXAFS, $\chi(k)$, is defined by the relation

$$\chi(k) \equiv \{\mu(k) - \mu_0(k)\}/\mu_0(k). \qquad 24.$$

Here, $\mu(k)$ is the experimentally observed absorption coefficient, while $\mu_0(k)$ is the smooth, monotonically decreasing portion of it. Figure 15 shows $\chi(k)$ for the previously illustrated $CuAsSe_2$ absorption, as obtained by Hunter (135).

Physically, the EXAFS arises in the following manner. The cross section for absorption of the photon is proportional to the square of the matrix element of the interaction, H_{int}, taken between the initial core

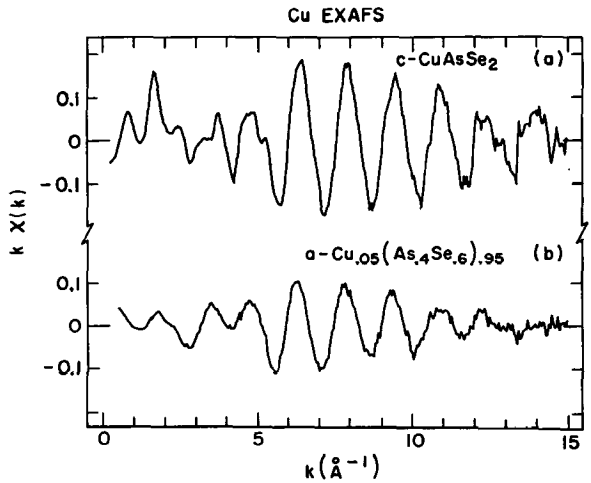

Figure 15 $k\chi(k)$ vs k for crystalline $CuAsSe_2$ and amorphous $Cu_{0.05}(As_{0.4}Se_{0.6})_{0.95}$ for the Cu absorption edge. Courtesy of S. Hunter, SSRL.

state, i, and the excited final state, f. The final state may be described as the sum of an outgoing wave with waves scattered by the atoms coordinating the photoexcited atom. Since the initial state, usually a K-shell state, is highly localized in the vicinity of a specific nucleus, this matrix element samples the form of the final state wave function in the vicinity of that nucleus. [For a discussion of EXAFS in which the initial state is an L state, see Lytle et al (141) and references contained therein.] This form is influenced by the interference between the outgoing and scattered waves. The interference depends strongly on the magnitude of the effective free electron wave vector of the photoemitted electron and the distance to the surrounding atoms. The change in k with changing photon energy, leading to the changing interference of outgoing and backscattered electrons, accounts for the oscillatory nature of the fine structure.

For K edges, the derivations of Sayers et al (139) as well as those of Ashley & Doniach (140) have led to a semiempirical equation for the $\chi(k)$ in terms of the atoms coordinating the specific species whose edge is being studied. It is

$$\chi(k) = -\sum_j (N_j/kR_j^2)\,|f_j(k)|\exp(-2k^2\langle u_j^2\rangle)\exp\{-R_j/\lambda(k)\} \times \sin\{2kR_j+\alpha_j(k)\}. \qquad 25.$$

Here, the summation is over coordination shells and atomic species within a shell, all denoted by the index, j. R_j is the average separation of atom j from the absorbing atom; $\langle u_j^2\rangle$ is the mean square deviation of that distance. The backscattering amplitude for the photoelectron from the neighbors is $|f_j(k)|$, N_j is the number of atoms in the shell at average distance R_j, $\lambda(k)$ is the energy dependent mean free path, and $\alpha_j(k)$ is twice the phase shift of the outgoing electron wave relative to the $1s$ core state together with the phase shift on backscattering.

Equation 25 implies that it is possible to determine the N_j, R_j, and $\langle u_j^2\rangle$ for each absorbing species in a complex, polyatomic material. These parameters constitute an almost complete description of the coordination of each species, and provide more information than is obtainable by any technique other than diffraction analysis of crystalline materials.

Since this equation is the basis of almost all attempts to use EXAFS to determine coordinations, it is worthwhile to review some of the important approximations associated with its derivation.

It is assumed, first of all, that the absorption process is dominated by a simple phenomenon in which a single core electron is promoted to an

excited state, while all the other electronic states remain essentially unchanged. It has become apparent, through the work of Kincaid & Eisenberger (146), Lee & Beni (143), and others that this simplification leads to an overestimate, by something between 30% and 100% of the magnitude of the EXAFS. As discussed by Rehr et al (submitted for publication), the discrepancies arise from two phenomena. First, even in this simple process, there is a relaxation of the surrounding electrons caused by the presence of the core hole. In addition, as the photon energy is increased above the edge, additional channels for absorption open up as the simultaneous excitation of one or more electrons in addition to the core electron associated with the edge (referred to as shake-up and shake-off) becomes possible.

They estimate that the first effect leads to a reduction to 0.60, 0.64, and 0.64 ± 0.04 for F_2, Cl_2 and Br_2, respectively, of the EXAFS magnitude predicted by Equation 25. They estimate that the second effect leads to an additional reduction on the order of 10% for these molecules. In addition, their theory of these effects indicates that the reduction factors should be quite sensitive to the nature of the local chemical environment of the absorbing atom. The consequences of this are discussed below. We note here, however, that uncertainties in the magnitude of these reductions lead to uncertainties in coordination numbers, N_j, determined by EXAFS analysis and are therefore very important.

In addition, it is assumed that single scattering dominates the scattering processes. That is, multiple scattering processes in which the photoexcited electron is scattered by more than one neighboring atom before "returning" to the excited atom are neglected. This approximation has been examined carefully by Ashley & Donaich (140) and by Lee & Pendry (144) for metallic copper. In addition, an exactly solvable one-dimensional model has been studied by Rehr & Stern (145). All three works lead to the conclusion that such multiple scattering cannot be ignored when attempts are made to determine coordinations beyond the first coordination shell, but that they are unimportant for first coordination shell determinations.

An important early test of Equation 25 was performed by Kincaid & Eisenberger (146), who measured the EXAFS spectra of gaseous Br_2 and $GeCl_4$, and calculated the relevant backscattering amplitudes and phase shifts in the static-exchange Hartree-Fock approximation. They showed that the theory predicts EXAFS roughly a factor of two larger than what they observed experimentally. In addition, there were disagreements of peak positions that were well outside their stated experimental error limits. They noted, "If one adjusts the starting value of the interatomic spacing, which is the most sensitive parameter in the theory, to improve

the peak-position agreement, the distance so determined is in error by 5%."

In associated work, Kincaid (147) presented two more results of particular importance in this context. The first was that the general shapes of the $|f_j(k)|$, and the values of the phase shifts, vary markedly with atomic number. The former have a peak as a function of k or $E-E_0$ approximately 100 eV above the edge for Cl, but 350 eV above the edge for Br. In general, the peak position moves to higher energy, and the peak itself becomes less pronounced, with increasing atomic number. This change of shape, which has also been noted by Lee & Beni (143), as well as the changes of phase imply that one should be able to identify the atomic constituents of each coordination shell observed if the discrepancies between theory and experiment can be resolved. Consequently, EXAFS analysis is a potential means of determining chemical ordering in amorphous materials and crystalline alloys.

In addition, Kincaid noted that the calculated backscattering amplitudes and phase shifts are quite sensitive to the many-electron approximation used. Consequently, some of the large difference between theory and experiment found by Kincaid & Eisenberger may be due to the inadequacies of the static-exchange Hartree-Fock approximation.

The absence of a complete theoretical basis for the analysis of EXAFS data coupled with clear experimental evidence of the insufficiencies of Equation 25, as well as the unavailability of reliable calculations of the backscattering amplitudes and phase shifts, mean that EXAFS analysis has been far from achieving the potential implied by Equation 25. In mature structure determination techniques, such as x-ray or neutron diffraction, there are a minimum of uncertainties in the theory and in important data analysis parameters like the scattering factors. Instead, the uncertainties are related to the atomic arrangements themselves. In EXAFS, on the other hand, the large uncertainties in the magnitude of the EXAFS, relative to the total absorption, and the smaller uncertainties in the phase shifts, have implied that structure analyses must necessarily lead to uncertain conclusions.

Consequently, two important lines of research have developed. One includes theoretical attempts to understand and calculate the spectra better. The other includes attempts to determine the backscattering amplitudes and phase shifts experimentally so that they may be used for structure determination. Included within this category are attempts to determine whether these parameters depend primarily on the atomic species being studied or whether, alternatively, they vary strongly from sample to sample even though the same elements are involved.

Initial emphasis in the latter line has been on the phase shifts, since

these play an important role in the determination of interatomic distances. This importance arises from the fact that they may be written, to a very good approximation, as

$$\alpha_j(k) = \alpha_{j0} + \alpha_{j1}k + \alpha_{j2}k^2. \quad 26.$$

Substitution of Equation 26 into the last factor of Equation 25 yields

$$\sin\left[2kR_j + \alpha_j(k)\right] = \sin\left[2kR_j + \alpha_{j0} + \alpha_{j1}k + \alpha_{j2}k^2\right] \quad 27.$$

Consequently, α_{j1} looks like an interatomic distance. Fourier transformation of the EXAFS yields peaks that are shifted from R_j by $\frac{1}{2}\alpha_{j1}$. All analysis techniques produce interatomic distances that are as uncertain as are the linear parts of the phase shifts. It is therefore important to determine the phase shifts reliably.

In an extremely important work, Citrin et al (148) established the transferability of phase shifts. That is, they showed that phase shifts associated with the absorption of a photon by a specific atomic species, A, and the scattering by a neighbor, B, in a known structure may be used to analyze the EXAFS from a system with unknown structure, where A is again the absorber and B the scatterer. Thus, even though there have only recently been theoretical calculations of phase shifts that might allow for such accuracy, experimental determinations of interatomic distances relying in one way or another on experimentally determined phase shifts have proceeded and have been accepted with some degree of confidence. Some of these are discussed in a later section.

More sophisticated theoretical calculations of phase shifts were recently published by Lee et al (149). These will constitute a substantial step forward in our ability to analyze data if, as anticipated, they prove to be generally reliable.

Similarly, more sophisticated theoretical calculations of backscattering amplitudes have been published by Teo et al (150). These, with the phase shifts, should aid considerably in the use of EXAFS to identify the chemical species surrounding the scatterer. Their immediate use in the determination of coordination numbers is limited, however, by the factors affecting the EXAFS amplitudes discussed above.

No comparable test of the transferability of EXAFS magnitudes from one system to another has been published. In view of the comments of Rehr et al discussed above, on the potential sensitivity of these magnitudes to chemical environment, such studies seem particularly appropriate. Lacking them, experimental determinations of coordination numbers must be accepted with caution.

7.2.3 DATA ACQUISITION Presented here is a brief discussion of the EXAFS measuring equipment presently being used by most experi-

mentalists at SSRL. Far more detailed descriptions have been presented by Kincaid (96) and by Hunter (135).

As shown in Figure 16, the x-ray beam from SPEAR passes through a Be window and a slit before it is monochromatized by successive Bragg reflections from the parallel faces of a channel-cut crystal located about 20 m from the source point. The beam then passes through ion chamber No. 1 for a measurement of the intensity incident on the sample, through the sample, and into ion chamber No. 2 for a measurement of the transmitted intensity. As the diagram indicates, the experiment is computer controlled. Although a complete analysis of the experiment is inappropriate here, some details will interest the general reader.

The long wavelength cutoff of this arrangement, determined by the thickness of the Be window, is presently about 3.5 keV. Efforts are under way to produce thinner windows, which will be consistent with the need for reliable isolation from the storage ring high vacuum.

The channel-cut crystal, when set to the Bragg angle for a specific wavelength, λ_0, may also pass $\frac{1}{2}\lambda_0$ and/or $\frac{1}{3}\lambda_0$. As Hunter discusses, this harmonic contamination decreases the accuracy of coordination number determinations, but not determinations of interatomic distances. This problem may be dealt with by maintaining the stored electron energy at a sufficiently low value so that the intensity of these harmonics is negligible. It is also possible, at many wavelengths, to choose a monochromator configuration that does not strongly reflect harmonics, or to suppress harmonics with mirrors.

Finally, as discussed by Hunter (135), the use of ion chambers in the configuration shown does not allow for an absolute measurement of the absorption coefficient. Instead, the absorption coefficient plus a slowly varying function of photon energy is measured. This fact must be taken into account in some applications of the data.

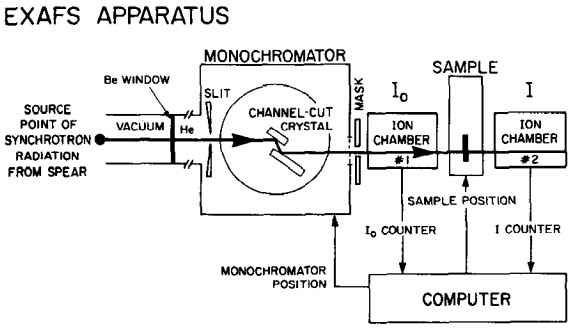

Figure 16 Block diagram of EXAFS experimental apparatus. Courtesy of S. Hunter, SSRL.

It should also be noted that the monochromatized beam emerges from the channel-cut crystal along a path parallel to, but displaced from, the original path. This displacement depends mostly on the crystal geometry and slightly on wavelength. Over the range of wavelengths in a typical EXAFS scan, the displacement of the monochromatic beam varies by about 1 mm or less. In some cases, this can be ignored. In other cases, the sample and detector system must be displaced to track the beam position.

7.2.4 DATA ANALYSIS Along with rapid developments in basic theory and data acquisition have come considerable advancements in data analysis, of which a very brief review is presented below.

As originally proposed by Sayers et al (139), Fourier transformation of the EXAFS data yields a radial structure function, $\phi(r)$, whose peak positions are shifted from the R_j as a result of the k dependence of the phase shifts, $\alpha_j(k)$, and whose peak heights and shapes are related in a complicated manner to the N_j and $\langle u_j^2 \rangle$. This complexity arises because of the shape of $|f_j(k)|$, the k dependence of the $\alpha_j(k)$, the presence of the Debye-Waller factor, and the finite region in k-space over which data is obtained, as discussed by Hayes et al (151, 152) as well as by Stern et al (153).

The Fourier transform, $\phi(r)$, of the Cu-edge EXAFS from crystalline $CuAsSe_2$ is shown in Figure 17. The first neighbor maximum is at 1.95 Å, whereas the interatomic distance is approximately 2.41 Å. Also shown

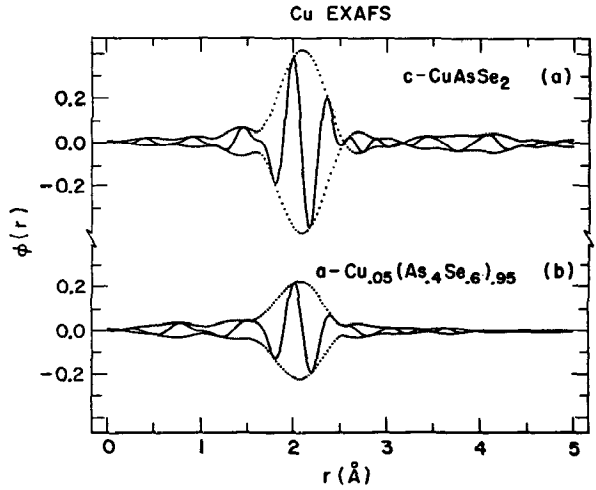

Figure 17 $\phi(r)$ vs r for crystalline $CuAsSe_2$ and amorphous $Cu_{0.05}(As_{0.4}Se_{0.6})_{0.95}$ from Cu-edge data. Courtesy of S. Hunter, SSRL.

is $\phi(r)$ obtained from the Cu-edge EXAFS from amorphous $Cu_{0.05}(As_{0.4}Se_{0.6})_{0.95}$, in which the Cu is also shown by Hunter et al (154) to be fourfold coordinated. Note that the peak height is much larger for the crystalline than the amorphous material. They show that this is because of the greater disorder in the amorphous material.

In the simplest analysis procedures aimed at determining coordination distances, the shifts in the peak positions due to absorber, A, and scatterer, S, are determined by using the $\phi(r)$ obtained from EXAFS studies of a sample in which the A-S interatomic distance is well known. Because of the complex factors that influence the peak shape, however, this approach may lead to small errors in interatomic distance. For this reason, more sophisticated methods have been developed.

These involve, in general, attempts to fit the contributions of the first or higher coordinations shells to the EXAFS or $\phi(r)$ with least squares or related analyses in which the r_j and $\langle u_j^2 \rangle$ are the parameters to be determined. Examples of these approaches are presented in References 142, 149, 150, 153, and 155.

7.2.5 EXAMPLES OF THE USE OF EXAFS FOR STRUCTURE DETERMINATIONS

Despite the brevity of the period in which EXAFS analysis and x-ray synchrotron radiation have been available, there are already more materials studied by this technique than can be described in such a review. To provide the reader with a slightly systematic summary, we concentrate, therefore, on four areas; (*a*) molecules of biological interest, (*b*) amorphous materials, (*c*) catalysts, and (*d*) surfaces.

7.2.5.1 *Molecules of biological interest* EXAFS analysis has been applied extensively to the determination of metal-ligand distances in molecules of biological interest. The applicability of EXAFS for studying crystalline materials is that it can be focused directly on the determination of the metal-ligand distances. In contrast, x-ray diffraction crystallographic structure determinations treat all the atoms in the unit cell equally, except for a weighting by the atomic number. Even the diffraction approach is unusable for many of these large molecules that have not yet been crystallized. In this case, EXAFS provides information unobtainable in any other way.

One of the most extensively studied proteins is rubredoxin, which has a molecular weight of approximately 6000 with one iron atom tetrahedrally coordinated by four cysteine sulphurs. Initial x-ray diffraction studies indicated that three Fe-S bonds were about 2.30 Å while the fourth was 2.05 Å (156). It was believed that appreciable strain energies were stored in the short bond.

EXAFS studies by Shulman et al (157), Bunker & Stern (158), Sayers et al (159), and Shulman et al (160) have shown that all four Fe-S distances are equal to within 0.10 Å. Consequently, the localized strain energy storage model does not seem to be applicable to this system.

Similar conclusions about the coordination of iron in different forms of hemoglobin have been drawn through the EXAFS studies of Eisenberger et al (161) as well as that of Eisenberger, Shulman, Kincaid, Brown & Ogawa available in preprint form. They have shown that the 3 kcal difference of oxygen binding energy between the high and low affinity forms of hemoglobin cannot be attributed to strain energy localized in the immediate vicinity of the iron atom. In addition, their determination of iron-nitrogen distances in oxy and deoxy complexes of hemoglobin also suggest that hemoglobin has a complex delocalized response to oxygen binding.

Several metal-containing molecules of biological relevance have been the subject of extensive EXAFS studies. Sayers et al (162) studied copper etioporphyrin I, Cramer et al (155) studied a number of iron porphyrins, while Kincaid et al (163) studied copper nickel tetraphenylporphyrin and methemoglobin. Hu et al (164) studied oxidized and reduced cytochrome c oxidase. Finally, the primary coordination environment of the "blue" copper iron in oxidized azurin has been determined by Tullius, Frank & Hodgson (preprint).

The coordination of Mo in various forms of nitrogenase has been investigated extensively by Cramer et al (165–167). This protein is important because of its role in bacterial nitrogen fixation. It is believed that the Mo is associated with the fixation site.

The reader may find a more detailed summary of the application of EXAFS to biological molecules in the review by Shulman, Eisenberger & Kincaid (preprint).

7.2.5.2 *Amorphous materials* Amorphous materials were among the very first studied by the Fourier analysis of EXAFS. Sayers, Stern & Lytle (139) presented an analysis of the data from crystalline amorphous Ge in 1971 and followed this by an analysis of amorphous Ge, GeO_2 and GeSe in 1972 (168) and of GeSe, $GeSe_2$, As_2Se_3, As_2A_3, and As_2Te_3 in 1973 (169). Among the contributions of this set of papers was the partial resolution of an important structural problem in the field of amorphous semiconductors, the coordinations of Ge and Se in amorphous GeSe. X-ray and electron diffraction radial distribution studies (170) of the amorphous germanium-monochalcogens had been unable to distinguish between two models for the atomic arrangements in these materials. In one, the germanium is fourfold coordinated while the chalcogen is two-

fold coordinated. In the other, each is threefold coordinated. The EXAFS work presented strong evidence for the first model. This model was rather important for understanding why many impurities have little effect on the electrical properties of amorphous semiconductors, as discussed by Mott (171).

More recently, Hunter et al (154, 172, 173) have studied an amorphous semiconducting system in which impurities have a drastic effect on the electrical conductivity, Cu in As_2Se_3. Using EXAFS, they were able to follow the changing coordination with copper concentration of the Cu, the As, and the Se separately. Similarly, Knights et al (142) have studied the coordination of arsenic impurities in amorphous silicon-hydrogen alloys. This work constitutes the first direct evidence for the occurrence of substitutional doping in an amorphous semiconductor.

Crozier et al (174) extended such studies of armorphous semiconductors into the liquid state in their analysis of the atomic arrangements in liquid As_2Se_3. The EXAFS data indicate that a major structural rearrangement does not occur in the nearest neighbor shell when As_2Se_3 is melted. These experiments, however, indicate small structural changes.

Finally, structural studies of the metallic glass $Pb_{78}Ge_{22}$ and sputtered amorphous $Pb_{80}Ge_{20}$ have been performed by Hayes, Allen, Tauc, Giesson & Hauser (preprint). The work indicates that the amorphous materials are chemically ordered, with each Ge being surrounded exclusively by Pb atoms. This result is important for understanding the formation and stability of metallic glasses.

7.2.5.3 *Catalysts* EXAFS has also been utilized extensively to determine the coordinations of metal atoms in catalysts. Its importance arises from the fact that the catalytic systems are often very finely dispersed, either on a support or in solution, so that normal x-ray diffraction procedures yield little information. EXAFS analysis yields the desired structural information, because it can be used to examine the average coordination of each metallic species in the catalyst. In addition, the valence state of the metals can often be determined.

In an early work, Lytle et al (175) used a standard x-ray tube to obtain EXAFS data from an alumina-supported CuCr catalyst. Cu is found to occupy both tetrahedral and octahedral sites in the supporting alumina lattice, while Cr was found only in octahedral sites. It was determined that the valence state was Cr^{+5} in the fresh catalyst, which changed to Cr^{+6} in the exhaust-cycled material. Confirmation of the valence state assignment was obtained by electron paramagnetic resonance.

Using similar experimental techniques, Bassi, Lytle & Parraveno (176) examined preparations of Au and Pt supported on Al_2O_3, MgO, and

SiO_2. The L_{III} x-ray absorption coefficient was normalized and Fourier-transformed to yield a radial structure function for each preparation. The analysis of the results showed that metals were present in two distinct phases: metallic with coordination (and metal-to-metal distance characteristic of bulk Au and Pt) as well as a highly dispersed one. It was concluded that the latter consisted of metal atomically dispersed or condensed in small, flat clusters of a few atoms. It was further estimated that the majority of Au and Pt was present in the highly dispersed form. The subsequent work described below was all performed at the Stanford Synchrotron Radiation Laboratory.

Lytle et al (177) examined the interaction of oxygen with a ruthenium-silica catalyst containing one weight percent ruthenium. Reed et al (178) studied the structure of the catalytic site of polymer-bound Wilkinson's catalyst. Reed & Eisenberger (179) studied the coordination of Rh and Pt in Bromo Tris(triphenylphosphine) rhodium(I). Reed, Eisenberger, Teo & Kincaid (preprint) studied the structural effects of cross linking in polymer-bound Bromo Tris(triphenylphosphine) rhodium(I) catalyst. Reed, Eisenberger & Hastings (preprint) studied the Ti-Cl bond distance in $TiCl_3$, a component in the Ziegler-Natta catalyst. Reed & Eisenberger (preprint) studied bond distances in $RhBr_3$ and Bromo Tris(triphenyl-phosphine) rhodium(I). Sinfelt et al (180) studied the coordination of platinum in two silica supported platinum catalysts as function of chemisorbed hydrogen.

In related work, Lytle (181) used the L_{III} x-ray absorption threshold to determine *d*-band occupancy in pure metals and supported catalysts, and to examine the correlation between percentage *d* character of the bulk metals and the catalytic activity of the supported metal.

7.2.5.4 *Surfaces* Studies of atomic arrangements on surfaces have been performed in two different ways with EXAFS. The simpler, in terms of technique, is to examine the EXAFS above the absorption edge of an atomic species adsorbed on a substrate that does not contain that species. The analyses by Stern et al (182, 183) as well as Heald & Stern (preprint) of bromine adsorbed on graphite are examples of these.

A second approach, examined in detail by Lee (184), involves the measurement of the intensity of the Auger emission line as a function of photon energy. Since the number of Auger electrons emitted is proportional to the number of photons absorbed at the surface, the measurement is essentially the same as measuring the x-ray absorption coefficient of the atoms at the surface and therefore the EXAFS. Citrin et al (185) determined directly the bond length and position of I adsorbed on the (111) face of Ag in this manner. These authors claim that this

approach, called surface-EXAFS (SEXAFS), offers three main advantages over low energy electron diffraction (LEED). It is easier to interpret, it is more accurate, and it does not require that the surface atoms be in a periodic array.

A related technique, described by Jaklevic et al (186) has been employed to measure the EXAFS spectrum from an atomic species present in very low concentrations in a material. Rather than measuring the transmitted radiation, the fluorescence radiation is counted as a function of incident photon energy. Since the fluorescent yield is expected to be a very slowly varying function of photon energy above the edge, the measurement is again an indirect measurement of the EXAFS associated with the fluorescing species. The gain in signal-to-noise is achieved by blocking out the fluorescent radiation from the other atomic species in the material. The authors demonstrate the power of the technique by showing EXAFS spectra from the Mn in a leaf, where it is present in concentrations of 10–50 ppm. They also show the As spectrum from a single crystal of Si doped with As at a concentration of $2\text{–}4 \times 10^{19}$ cm^{-3}. This method was also employed by Shulman et al (160) in their study of rubredoxin. The concentration below which fluorescence gives better results than transmission depends on several factors, particularly the edge energy. For example, for energies below about 7 keV and concentrations below 10 millimolar in the metal atom, fluorescence is the preferred method.

7.3 *X-Ray Fluorescence—Trace Element Analysis*

The repopulation of an electron core level vacancy in an atom can result in the emission of characteristic fluorescence radiation, which can serve as a tag of the particular element and thus provide the basis of quantitative element identification. The creation of core level vacancies can be accomplished by exposing the sample to sufficiently energetic proton, electron, or electromagnetic radiation. All of these are used in trace element analysis work. The advantage of photons as the exciting radiation lies in their relatively high absorption cross section and relatively low cross section for scattering.

As a source of photons, synchrotron radiation has several favorable characteristics, particularly its high intensity, broad bandwith (which permits wavelength selection near absorption edges), and high collimation (facilitating the efficient use of focusing crystals to produce very small area beams of monochromatic radiation). Furthermore, the high linear polarization of the radiation, with its **E** vector in the plane of the electron acceleration means that the Rayleigh (elastic) and Compton (inelastic) scattering goes through a minimum in the direction of this **E** vector. Thus, a detector placed in this location will have much reduced back-

ground without decrease in the intensity of the isotropically emitted fluorescence radiation.

All of these properties have been very effectively used in an experimental search for super-heavy elements by Sparks et al (187, 188) at SSRL. Their experimental arrangement is shown in Figure 18, and typical fluorescence spectra are shown in Figure 19. The hot-pressed curved pyrolytic graphite (mosaic spread 0.4°) monochromator collected 2 mrad of synchrotron radiation in the horizontal plane and 0.14 mrad (about half of the total vertical divergence at 37 keV) in the vertical plane, which produced a focused flux of about 4×10^{10} photons per sec-mm^2 at 37.5 keV [300 eV full width half maximum (FWHM)] with SPEAR operating at 3.4 GeV and 20 mA. By tuning the monochromator, photon energies can be selected to bracket an absorption edge (in this case the L edge of element 126). Thus, a high degree of confidence can be obtained in any observed signal.

No evidence for the existence of super-heavy elements was found in a variety of samples, including monazite inclusions in mica crystals in which an earlier proton-induced fluorescence experiment (189) had reported possible evidence. The synchrotron radiation experiments had a sensitivity sufficient to observe about 5×10^8 super-heavy atoms per sample—about 55 times higher sensitivity than the proton experiment. Further refinements in the technique and higher incident fluxes should make it possible to detect concentrations as low as 10^6 atoms per sample (C. J. Sparks, private communication).

In the Soviet Union, trace element concentrations of $2–3 \times 10^{-8}$ g/g have been observed in samples of petroleum, powdered minerals, and salt solutions using the VEPP-3 storage ring in Novosibirsk (190). Concentrations of 10^{-7} g/g could be detected in 100 sec.

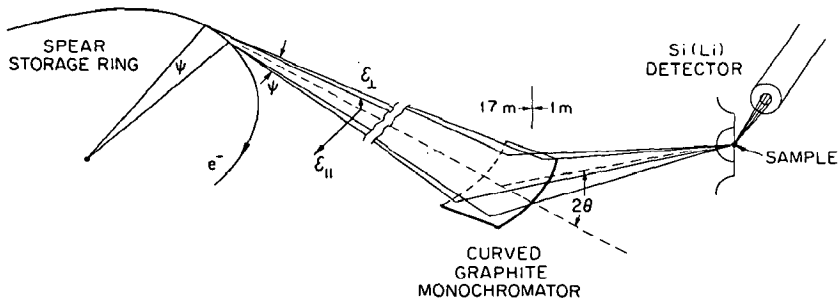

Figure 18 Schematic layout of Oak Ridge National Laboratory experiment used in the search for superheavy elements (188). Courtesy of C. J. Sparks, Oak Ridge National Laboratory.

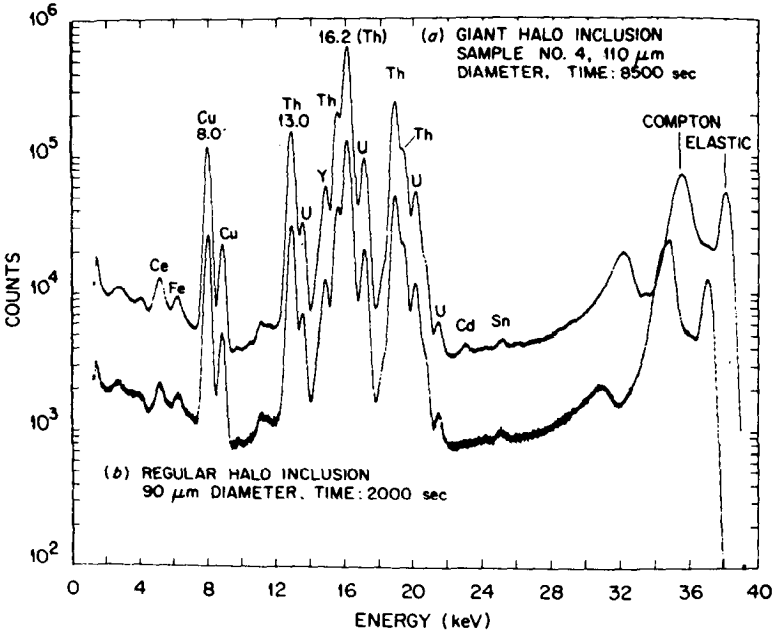

Figure 19 Typical fluorescence spectra obtained in the superheavy elements search (187). The L emission lines from superheavy elements, if present, would appear in the 22–31 keV region. The Cd and Sn peaks are due to trace quantities of these elements in the sample, sample chamber, or detector. The peak labeled Cd in the upper curve is due to the presence of about 5×10^9 atoms of cadmium in the sample. Courtesy of C. J. Sparks, Oak Ridge National Laboratory.

7.4 *X-Ray Lithography—Microstructure Replication*

The replication of patterns with micron- and submicron-sized features (such as integrated circuit patterns) by x-ray lithography is a new technique, begun in 1972 with the pioneering work of Spears & Smith (191) using conventional x-ray generators. The qualities of synchrotron radiation (e.g. high intensity, natural collimation) for this purpose were clearly demonstrated in the experiments of Spiller of IBM and collaborators in 1976 using the DESY synchrotron (192) and also by a group from the Thomson–C.S.F. Company and Orsay in 1976 using the ACO storage ring (193). A comprehensive review of x-ray lithography has recently been produced by Spiller & Feder (194).

The industrial interest in x-ray lithography using synchrotron radiation is increasing very rapidly. In both Germany and France, provisions have been made for private companies to use government-operated synchrotron radiation facilities for research and development work in

x-ray lithography, including proprietary work. In some cases, production of devices is also anticipated. In the US, where there are greater restrictions on proprietary work at government-sponsored laboratories, a private company, the Electron Storage Ring Corporation in San Francisco (195) has been formed to build a privately owned storage ring for x-ray lithography and other commercial applications of synchrotron radiation.

The x-ray lithographic process consists of the following steps:

1. A mask containing a pattern is placed in close proximity to a wafer (normally silicon) overcoated with a thin layer of x-ray sensitive material called a photoresist—generally an organic polymer.
2. The photoresist is exposed through the mask to an x-ray beam. If the mask pattern consists of x-ray absorbing material (e.g. gold) on a thin backing film (e.g. mylar), then x rays are transmitted only where there is no absorber. The transmitted x rays cause chemical changes in the photoresist (e.g. they break bonds in long chain polymers).
3. The photoresist is developed in a solvent that removes exposed and unexposed regions at a different rate. Thus, the pattern of the mask is replicated in the photoresist.

Subsequent processes (e.g. plating, diffusion, ion implantation) are used to transform the pattern into an integrated circuit, a memory device, or other microstructure. Often successive exposures overlaying several different patterns with processing steps between exposures are required to make a single device. Precise registration of these different exposures is necessary to a tolerance of a fraction of the size of the smallest linewidth or feature.

The steps described above are basically the same whether x rays or more conventional radiation sources (visible or UV light, electrons) are used. However, x rays have several distinct advantages over the others, particularly in the replication of submicron structures. Briefly, these advantages are: (*a*) Short wavelength (10–50 Å) reduces diffraction effects. This makes possible the replication of structures with line-widths ~ 0.1 μm. With visible and UV light, diffraction limits linewidth to ~ 1 μm. (*b*) Mask need not be in direct contact with wafer. This increases mask life. (*c*) Relative insensitivity to dust. (*d*) Deep parallel grooves with large aspect ratios can be made (see Figure 20). (*e*) High intensity available with synchrotron radiation makes possible short exposure time (~ 1 sec) even with high resolution, low sensitivity photoresists such as polymethylmethacrylate (PMMA).

In the Soviet Union, x-ray lithographic work has been done using the VEPP-3 storage ring in Novosibirsk (196). Patterns were recorded

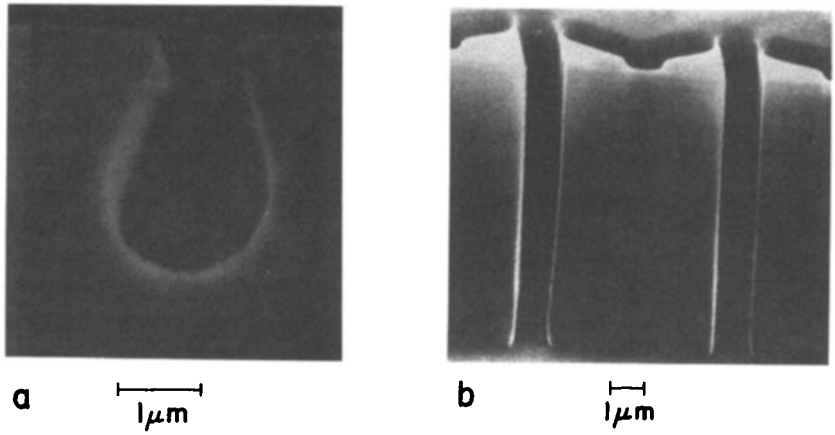

Figure 20 Comparison of grooves made by (*a*) electrons of 15-keV energy [Courtesy of M. Hatzakis, IBM, Yorktown Heights, NY (256)] and (*b*) x rays of 2.5-keV energy [Courtesy of E. Spiller, IBM, Yorktown Heights, NY (194)].

on chalcogenide glass films, producing a direct change in index of refraction without the need for development.

It appears likely that, with the increased availability of synchrotron radiation sources, particularly to industrial users, the technique may become developed and perfected to the extent that it will have a major impact on the semiconductor industry and other areas of microstructure fabrication. Examples of structures that have been fabricated using x-ray lithography are given in Figure 21.

7.5 *X-Ray Microscopy*

There is a growing interest in the application of synchrotron radiation to x-ray microscopy. Since 1972 three quite different x-ray microscopes have been built and operated using synchrotron radiation. Sayre et al (197) reviewed soft x-ray microscopy. Kirz et al (198) made a comparative analysis of x-ray emission microscopies for biological specimens using incident proton, electron, or x-ray beams focused to a small spot. They conclude that radiation damage limits the resolution for unstained biological specimens and that incident x-ray beams give the lowest dose for elements with atomic number above about 10.

We now discuss the three types of microscopy that have been demonstrated with synchrotron radiation.

7.5.1 SCANNING X-RAY MICROSCOPY The principal of operation of this device, as implemented by Horowitz & Howell (97) in 1972, is shown in Figure 22. Synchrotron radiation from about 10 mrad of orbit from the

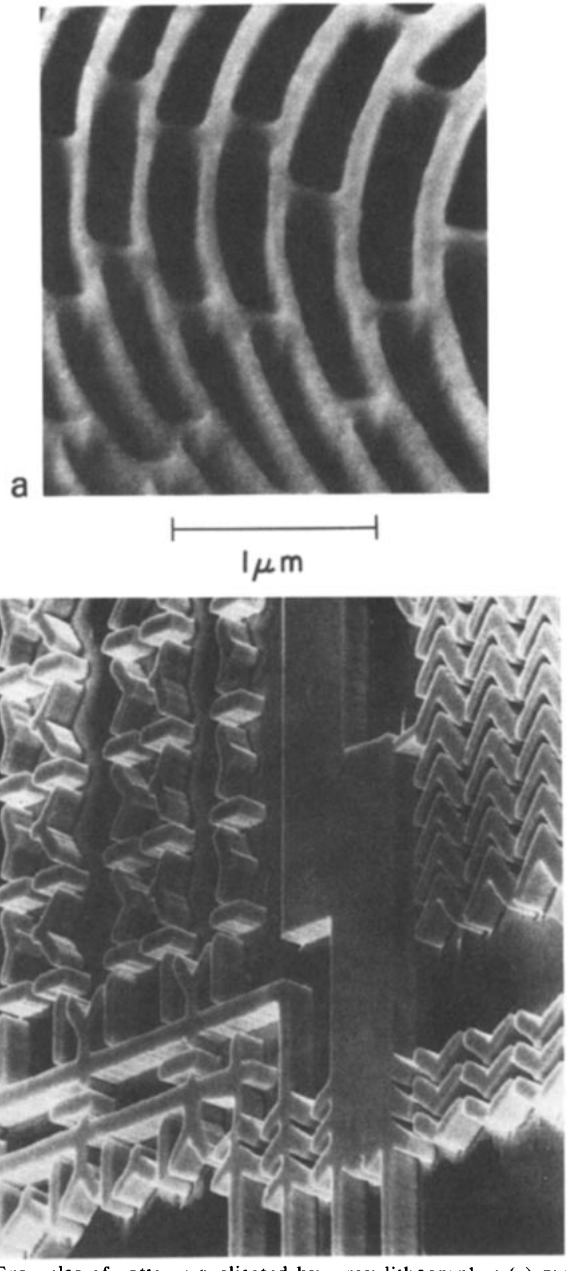

Figure 21 Examples of patterns replicated by x-ray lithography: (*a*) zone plate pattern and (*b*) magnetic bubble memory pattern. The individual features are 1 μm wide and 3 μm high for the bubble memory pattern. Courtesy of E. Spiller, IBM, Yorktown Heights, NY (194).

CEA storage ring was collected at grazing incidence, totally externally reflected, and focused by a quartz ellipsoidal mirror. Just upstream of the focus, the synchrotron radiation passed through a very thin (10 μm) beryllium foil, which terminated the high vacuum beam run. The focused x-ray beam was so intense that upon emerging from the beryllium window, it caused a readily visible air fluorescence as shown in Figure 23 (with the microscope removed). The focal spot was roughly 1×2 mm^2, but this was further collimated by a 2-μm pinhole in a 100-μm gold absorber foil.

The sample, which could be in an air or helium atmosphere, was scanned raster (line by line) fashion across the resulting 2-μm-sized beam. Fluorescent x rays, produced by the part of the sample being irradiated, were detected, energy analyzed, and the resulting signal used to intensify the beam of a cathode ray tube that was being swept synchronously with the sample. The main features of the microscope are the following (97): (*a*) The sample could be in air or other atmosphere, which facilitates the study of hydrated, even live, biological specimens. (*b*) A resolution of $\sim$2 μm can be obtained, determined by the diameter of the pinhole. (*c*) The depth of field was about 1 mm, which facilitates stereoscopic viewing of pictures taken at different angles. However, the x rays penetrate 10–100 μm of most material. (*d*) It is possible to select a given element whose absorption edge is in the range of the instrument and determine the distribution of that element in the sample. The condensing mirror provides a cutoff above about 3.5 keV, and the beryllium window absorbs strongly below about 1 keV. (*e*) It takes about two minutes to form a picture.

The development of this microscope with synchrotron radiation

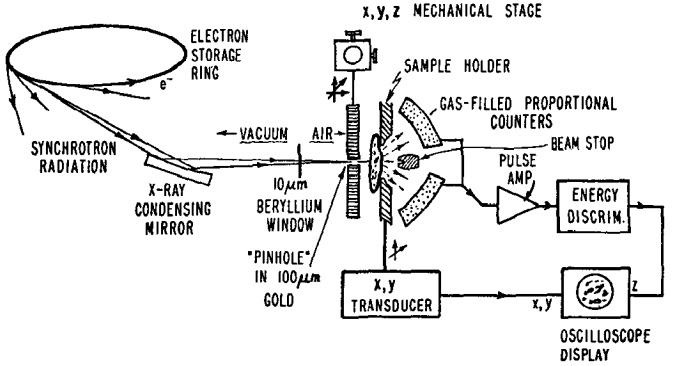

Figure 22 Schematic of scanning x-ray microscopy using synchrotron radiation. Courtesy of P. Horowitz, Harvard University.

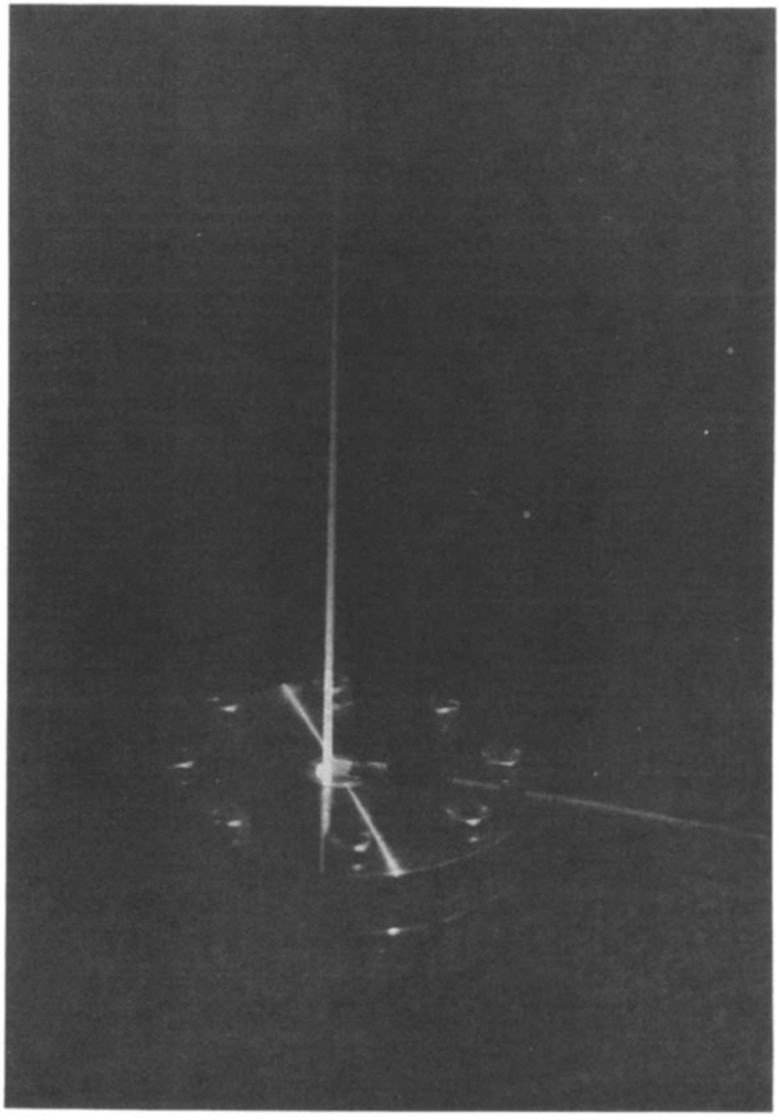

Figure 23 Focused x-ray beam from CEA storage ring emerging from beryllium window and causing visible air fluorescence. Courtesy of P. Horowitz, Harvard University.

terminated in June 1973, when the CEA was shut down. The instrument has since been continued as a proton microprobe (199).

7.5.2 ZONE PLATE X-RAY MICROSCOPY Using synchrotron radiation from the DESY synchrotron, Niemann, Rudolf & Schmahl (200) operated the zone plate microscope shown schematically in Figure 24. The incident white synchrotron radiation is dispersed at grazing incidence by a reflection grating. A focal spot of monochromatic light is produced onto the sample by the first zone plate, which has a 5-mm diameter, 2600 zones, and a focal length of 522 mm for 46 Å radiation. A second zone plate with a diameter of 1 mm, 850 zones, and a focal length of 64.5 mm for 46 Å radiation forms a magnified image of the object. In their first tests, a resolution of 0.5 μm was obtained, and several biological objects were examined. Work is in progress to improve the resolution, reduce the exposure time (now some minutes long), and to study other samples (200).

7.5.3 CONTACT X-RAY MICROSCOPY Using a technique quite similar to x-ray lithography, a collaboration of scientists from IBM, DESY, NYU Medical School, and Yale University have obtained contact x-ray micrographs of biological objects with very high resolution (201). Both synchrotron radiation and carbon K_α x rays were used.

The specimen to be examined is placed in direct contact with a photoresist and exposed to the x rays (see Figure 25). The absorption profile of the specimen is recorded in the photoresist, which is then developed, coated with a metal film, and examined in a scanning electron microscope.

The highest resolution ($\sim$100 Å) was obtained using broadband synchrotron radiation with wavelengths in the range of about 30–44 Å. For

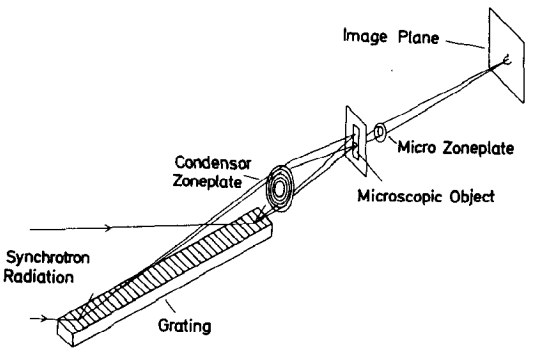

Figure 24 X-ray microscopy using zone plates. Courtesy of B. Niemann, Universitäts-Sternwarte, Göttingen (200).

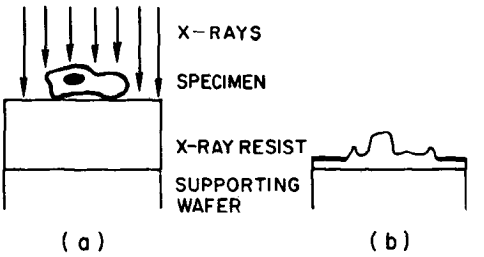

Figure 25 Schematic of contact x-ray microscopy technique. Courtesy of E. Spiller, IBM, Yorktown Heights, NY (201).

shorter wavelengths, the resolution is poorer because secondary electrons have a longer range in the photoresist. For longer wavelengths, diffraction limits the resolution. Some results are shown in Figure 26, which includes a scanning electron micrograph for comparison. The figure shows that the x-ray micrographs reveal the interior structure, while the scanning electron micrograph exhibits only surface structure.

A collaboration from the University of Paris and the Orsay Synchrotron Radiation Laboratory (202) performed similar measurements using monochromatized synchrotron radiation. By selecting incident photon energies corresponding to particular elemental absorption edges, they were able to do chemical microanalysis with a resolution of a few micrometers.

7.6 *Ultraviolet and Soft X-Ray Studies of the Electronic Structure of Matter*

7.6.1 INTRODUCTION Compared to its utilization in the x-ray portion of the spectrum, vacuum ultraviolet (VUV) radiation research utilizing synchrotron radiation is a well-established field with a vast primary literature and several fine recent review articles (42, 203–215). Because this field has been reviewed so extensively and well, we present here a brief overview of the types of studies being performed, with references to recent reviews containing more detail.

The basic utility of VUV for exploring electronic states arises from the fact that the photon energies range from 10^1 to 10^3 eV. That is, the photon energies cover the range of binding energies from deep valence states to many core states. Consequently, the basic experimental approaches—reflection, absorption, fluorescence, and photoemission—provide valuable information about the nature of those electronic states and related collective excitations (plasmons, excitons, etc). At the same time, research in this field must necessarily be concerned with obtaining

increased understanding of the interaction between the electromagnetic radiation and the substances being studied.

In performing VUV experiments, synchrotron radiation offers a number of advantages over other sources. As in most of the x-ray experiments, the most important feature is that high intensity is obtained over a continuous spectral range. That is, one need not be constrained to the use of characteristic radiation to obtain high intensity. It is quite apparent

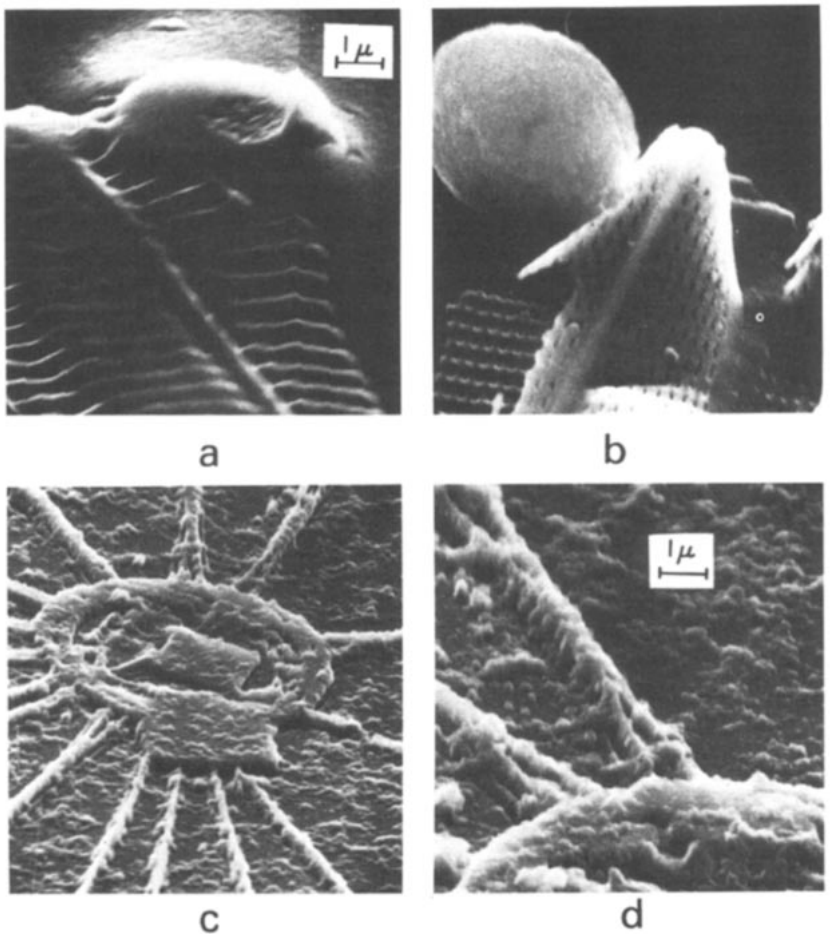

Figure 26 X-Ray replicas of diatoms (*a*, *c*, *d*) and scanning electron micrograph of a diatom (*b*). In (*a*) the x-ray source was carbon K_α radiation and the exposure time was 20 hr with a source-to-specimen distance of 15 cm. Part (*d*), a detail of (*c*), was taken with synchrotron radiation in 10 min with the specimen 40 m from the source. Courtesy of E. Spiller, IBM, Yorktown Heights, NY (201).

that this feature facilitates absorption and reflection measurements as a function of photon energy. Less obvious is that it allows the probing of electronic states as a function of depth in the photoemission experiment, as discussed below. This feature has led to the rapid growth of surface studies and studies of sorbed gases through photoemission in recent years, as discussed by Spicer (214).

Of equal importance to such studies is the fact that the electron storage ring is a high vacuum source, hence it does not contaminate the surfaces being studied. The high intensity also makes possible photoemission experiments in which the electron yield is sufficiently high to perform angle-resolved photoemission experiments. Similarly, there is the fact that a flat "pancake" of radiation is produced with very little dispersion away from the plane of the electron orbit. This lack of dispersion is very important because it allows the radiation to be collimated with much less loss than that given by more divergent sources. Finally, another important characteristic of the radiation is its natural linear polarization in the plane of the electron orbit. This can be particularly important for studies involving optical selection rules and/or angularly resolved photoemission.

A particularly active area of research has been the study of the optical properties of metals and semiconductors. This research is particularly timely because band structure calculations can now provide fairly good representations of the one-electron theory predictions of these optical properties. Of particular importance in these analyses are the modulation spectroscopy techniques—electroreflectance, thermoreflectance, and wavelength modulation—made possible in the region above 10 eV by the intense, continuous, and stable synchrotron radiation available from electron storage rings. These techniques enhance weak structure in the optical spectra, emphasizing the contributions of localized regions in the Brillouin zone, such as critical points, and have been particularly effectively utilized at the Synchrotron Radiation Center in Wisconsin.

While data so obtained are important in the analysis of band structure and the testing of band structure calculations, it has been apparent for some time that not all of the spectral features can be treated within the one-electron, Bloch-type theory, so there is a strong interaction between these experimental studies and many-electron theory.

Much of the experimental work and its relation to theory has been described well by Brown (207), by Haensel (209), and by Koch et al (213). Lynch's review article (216) emphasizes the relationship between existing theory and experiment for metals, while that of Aspnes (217) deals with semiconductors. Mahan (218) has provided an excellent description of the many-body theoretical treatments of the VUV and x-ray optical properties of metals.

Another area that has advanced considerably as a result of synchrotron radiation is the use of VUV photoemission to probe the electronic structures of bulk solids, as well as surfaces. At the same time, the photoemission process itself has been the subject of considerable study. In these experiments, a monochromatic beam incident upon the samples yields photoemitted electrons. In many experiments, the total yield is measured as a function of photon energy. In energy-resolved photoemission, however, the energy distribution of the photoemitted electrons is determined as a function of photon energy. From such measurements, information about the densities of initial and final states can be obtained. If, in addition, angle-resolved photoemission studies, in which the direction of emission is also analyzed, are performed, information about the form of the initial and final states involved in the photoexcitation may be obtained. These energy- and angle-resolved studies, which involve a small portion of the total photoelectron yield, have benefited greatly from the high intensity of synchrotron radiation.

7.6.2 CROSS-SECTION EFFECTS Examples of fundamental studies of the photoemission process are the studies of energy dependent cross sections, which take advantage of the tunability of the synchrotron radiation. Cooper & Fano (219, 220) predicted minima in the atomic photoemission cross section if the initial state wave function exhibits a radial node. This effect has been studied (215, 221, 222) for the *d*-band intensity in the noble metals Cu (3*d*, no radial node), Ag (4*d*, one radial node), and Au (5*d*, two radial nodes), as well as for In and Sb (223, 224). As shown in Figure 27, the energy dependence of the *d*-band intensity, which is proportional to the photoionization cross section (222), is significantly different for the three noble metals. Above threshold, the intensities first exhibit maxima that occur in the order Au 5*d* (<40 eV), Ag 4*d* (~ 60 eV), and Cu 3*d* (~ 130 eV). This is due to an increasing overlap of the *d*-initial and *f*-final state wavefunction (the $d \rightarrow f$ channel dominates the $d \rightarrow p$ one above ~ 20 eV). This overlap is small above threshold where the *f*-wave is pushed out by the centrifugal barrier, but it increases at higher energies in the order $5d > 4d > 3d$, the order of decreasing radial expectation values of the *d*-orbitals. At still higher energies, the *d*-band intensity decreases steeply to a minimum for Ag and Au. These so-called Cooper minima arise from a change of sign in the radial dipole matrix element associated with the $d \rightarrow f$ channel. The photoexcitation cross section, which is proportional to the sum of the squares of the *p* and *f* channel radial matrix elements, will exhibit a minimum at the energy for which one of the matrix elements vanishes. As compared to the 4*d* function in Ag (one node), the 5*d* function in Au has two nodes and the Cooper minimum is smeared out. These minima have important consequences

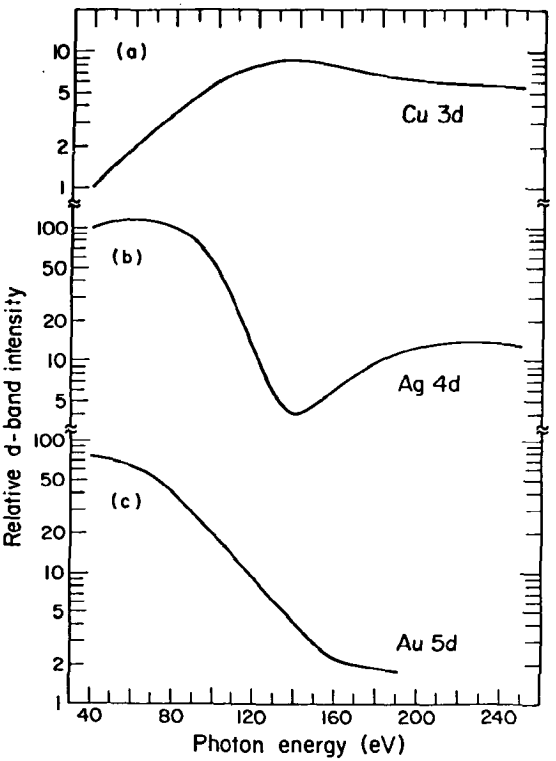

Figure 27 Relative *d*-band intensity vs photon energy for Cu 3*d*, Ag 4*d*, and Au 5*d* (221).

for the utilization of photoemission in the study of adsorbates on 4*d*- or 5*d*-type metals, as discussed below.

By tuning the photon energy to the Cooper minimum of the metal, a significant enhancement of the relative absorbate spectral intensity is achieved.

7.6.3 BAND STRUCTURE EFFECTS Photoemission has been used for many years to probe the band structure of solids. In these studies, the availability of synchrotron radiation has had two important consequences. First, the exciting photon energy may be varied continuously over a very large range, with a resultant variation in the relationship between the initial and final states involved in the process. This variation has allowed for more detailed determinations of the densities of states involved. Second, as discussed above, the high intensity has facilitated the development of energy- and angle-resolved photoemission. Thus the information

obtained has become still more definitive. Recent work is reviewed by Koch et al (213), by Eastman (225), and by Shirley et al (215).

7.6.4 SURFACE AND ABSORBATE EFFECTS An entire line of research that owes its existence very much to the availability of tunable synchrotron radiation, and that is also of considerable current theoretical and practical interest, is the study of structure and electronic states of surfaces and of absorbates on surfaces, as reviewed by Lindau (226), by Shirley et al (215), by Spicer (214), as well as by Plummer & Gustafsson (257).

The importance of a tunable source can be understood through reference to the plot (227) of the electron escape depth as a function of the electron energy above the Fermi level for a large number of materials shown in Figure 28. This depth has a minimum of the order of a few

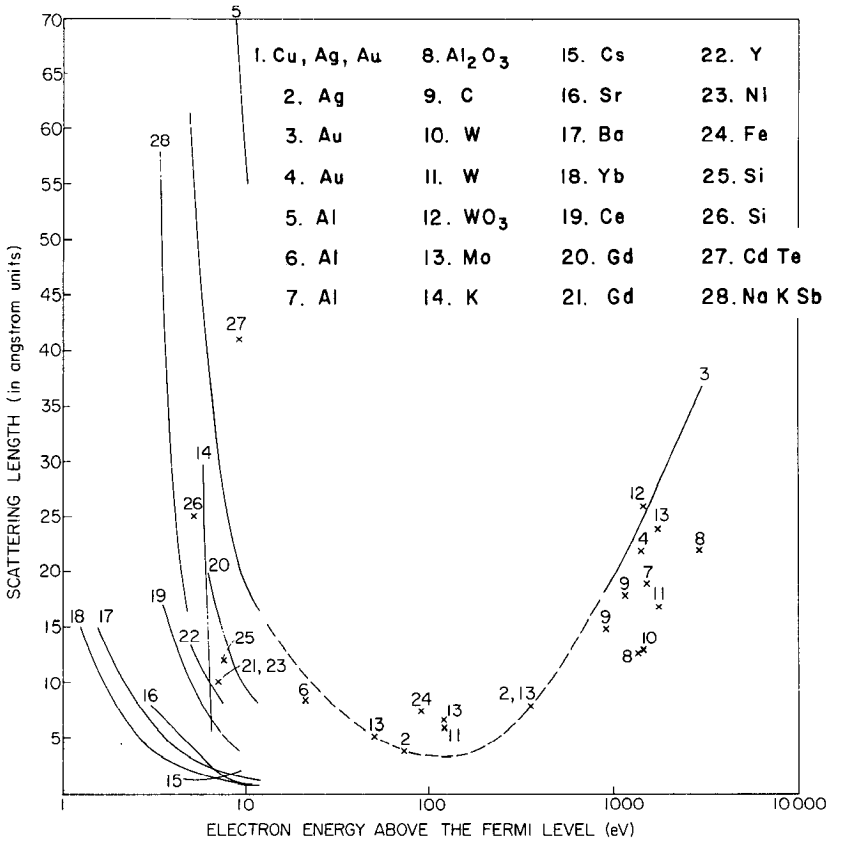

Figure 28 The escape depth, in Å, is shown as a function of the electron energy above the Fermi level, in eV, for a large number of materials (227).

angstroms at energies that range from ten to a couple of hundred eV, depending on the material. To study core electronic states of surfaces or of absorbates, one may tune the incident photon energy so that electrons photoemitted from a specific core level have energies close to the minimum. As a result, few electrons excited from the bulk of the material escape, and hence those detected are primarily from the surface or from the absorbate. Alternatively, in studies of absorbates on appropriate substrates the photon energy can be tuned to the Cooper minimum of the substrate, so absorbate emission dominates the detected electrons.

These studies are of considerable theoretical interest since methods for calculating the electronic states at the surface of solids are now being devised and employed actively. In addition, they are of considerable practical importance for the understanding of semiconductor surfaces, semiconductor passification, and catalytic activity. The reader interested in the latest work in this rapidly developing area is referred to the reports of the users' meetings of the Synchrotron Radiation Center at Wisconsin (228) and the Stanford Synchrotron Radiation Laboratory (229).

Finally, we should call attention to the very recent work of Stöhr, Denley & Perfetti (preprint) as well as Bianconi & Bachrach (preprint) in which SEXAFS studies have been performed through the measurement of inelastically scattered photoelectrons as a function of photon energy. Stöhr et al determined the O-Al near neighbor distance on an oxidized Al surface, while Bianconi & Bachrach measured the Al-Al distance on a clean Al (111) surface.

7.7 *Time-Resolved Spectroscopy Using Synchrotron Radiation*

The pulsed time structure of synchrotron radiation is very well suited to a variety of applications in time-resolved spectroscopy (TRS). The first TRS using synchrotron radiation excitation was done in 1974 by López-Delgado, Tramer & Munro at ACO in France (230). Several studies of time-resolved excitation, emission, and decay of excited states in organic and inorganic molecules have resulted from this work (231, 232). Nevertheless, the relatively short (73 nsec) interpulse period and rather broad pulse width ($\sim$1 nsec) available at ACO prevented those investigators from studying very short and very long lifetimes. The time structure of synchrotron radiation at SSRL from the SPEAR ring with its 300-psec pulse width and 780-nsec interpulse period, enabled López-Delgado, Miehé & Sipp (233) to measure fluorescence decay times as short as 0.2 nsec in tetracene crystals. A review of TRS techniques and results has been given by López-Delgado (234).

Several TRS experiments have since been done at SSRL (235). Matthias, Shirley, and co-workers have investigated fluorescence lifetimes in noble gases and simple molecules (236). Of special significance is their use of the polarization of synchrotron radiation to observe quantum beats in the fluorescence from magnetically oriented atoms (237). Simultaneously, Monahan & Rehn have been studying exciton-enhanced energy transfer in the pure and doped noble solids (238, 239). These investigators have demonstrated that TRS using synchrotron radiation can be used to determine the principal channels of energy transfer and their relative importance in these systems. This work has been highlighted by the discovery of previously unobserved electronic states, excimer (i.e. a diatomic molecule with one or more bound excited states and a repulsive ground state) species, and dissociation phenomena (239, 240).

The application of TRS techniques at SSRL and throughout the world are on the increase. A visible light and near-UV TRS port on the SPEAR ring was made operational in early 1978, and plans are being made to install a VUV port with large acceptance angle. Hahn, Jordan & Schwentner (241) have done some preliminary lifetime studies at the DORIS storage ring in Germany and are planning a number of experiments when DORIS is converted to single-bunch operation ($\sim$1-μsec period). In addition, storage rings in Novosibirsk have time structure suitable for TRS, and work in this area is expected in the near future. Many of the new storage rings now under construction as dedicated synchrotron radiation sources will be capable of operating in multibunch mode for maximum synchrotron radiation intensity and also single-bunch mode to facilitate timing studies.

7.8 *Applications in Atomic and Molecular Physics*

The continuous spectrum feature of synchrotron radiation, coupled with its high intensity, offers the opportunity, largely unexploited, for a vast array of experiments involving the interaction of electromagnetic radiation with atoms and molecules. One set of experiments, however, makes clear the powerful potential.

Ice & Crasemann (242) measured the differential cross sections for the total scattering of photons by H_2 at large momentum transfer. Such cross sections are of interest because total x-ray scattering is a two-electron expectation value, whereas coherent (elastic) intensity is a one-electron property (243). Thus, coherent scattering is routinely used to determine radial charge density distributions, i.e. the expectation of the electron-nucleus separations. The inelastic scattering intensity, on the other hand, is sensitive to electron correlation and depends upon the

expectation of the inverse the electron-electron separation, $\langle r_{ij}^{-1} \rangle$. Of considerable interest in this regard are the two-electron systems H_2 and He. Because the cross sections are very small, of the order of hundreds of millibarns per steradian, they cannot be measured with adequate accuracy using ordinary x-ray sources.

In experiments now underway on neon, Ice, Parente & Crasemann (G. E. Ice, private communication) are utilizing the tunability of synchrotron radiation to perform a more sophisticated version of this experiment in which the elastic part of the scattering is experimentally removed. The motivation for this work is that the inelastic scattering is much more sensitive to the scattering model and the wave functions than is the elastic. Experimental removal of the elastic scattering provides a more direct and accurate measurement of the inelastic scattering.

This is achieved by using incident photons whose energies are a few eV higher than an absorption edge of an absorbing element placed between the scatterer and the detector. Consequently, the element absorbs heavily the elastically scattered radiation, but for most momentum transfers is relatively transparent for the inelastically scattered x rays, whose energies are below the edge. These then reach the detector and are counted. Such a technique is possible with a highly tunable x-ray source but is generally impossible with standard sources.

7.9 *Some Future Applications*

7.9.1 PUMPING OF X-RAY LASERS Synchrotron radiation offers probably the most promising approach to achieve the high spatial and temporal energy densities required for pumping an x-ray laser (244). Furthermore, the ability to select any desired photon energy from the synchrotron radiation continuum is a major advantage. By selecting an energy just above the K edge, a much higher fraction of the incident energy results in pumping the desired level with corresponding reduction in unwanted ionization and heating of the medium. Since the lasing material remains relatively cool, and ionization is relatively low, homogeneous and inhomogeneous line broadening will be small, which thus enhances laser action. In addition, in a cool plasma, the outer electron structure of atoms can be rearranged by resonant transitions induced by low energy photons, and one is no longer restricted to configurations common in nature.

For example, a small volume of Li gas of 5×10^{18} cm^{-3} density irradiated with 1.8-eV photons from a conventional laser as well as with x rays just above the K edge of Li can be made to lase at 90 eV with about 100 times the photon pumping intensity now delivered by SPEAR in this energy range (244). The required intensity is likely to be reached

with wigglers and with high current, low emittance dedicated operation of SPEAR and other storage rings.

7.9.2 X-RAY HOLOGRAPHY WITH SYNCHROTRON RADIATION: COHERENCE The coherence properties of synchrotron radiation are superior to those of conventional x-ray sources, a feature that should greatly facilitate x-ray holography. For example, for VEPP-3, the power useful for holography has been calculated to be three orders of magnitude greater than the coherent radiation power from x-ray tubes (245).

Using such a source and a MWPC detector, it should be possible (50) to obtain x-ray microholograms with 1 Å incident radiation with a resolution of 50 Å transverse and 2500 Å longitudinal. The calculated exposure time is 1 sec.

Considerably higher coherent power would be available from a free electron laser (see Section 5.3) if such a device could be made to operate at the required photon energy and in a storage ring. It has also been suggested that synchrotron radiation could pump x-ray lasers (see previous section), which would be powerful sources of coherent x rays.

Lensless Fourier-transform x-ray holograms of simple one-dimensional objects have been obtained (246) with carbon K_α radiation (44.8 Å) and with synchrotron radiation (60 Å) (247). Two- and three-dimensional objects have also been studied (248) with aluminum K_α radiation (8.34 Å) with a resolution of 4 μm transverse and 4 mm longitudinal and with exposure times of $\sim$1 hr.

By recording a hologram at one wavelength and reading it at another wavelength, a magnification corresponding to the ratio of the wavelengths may be obtained. Csonka (249, 250) recently analyzed the application of synchrotron radiation to x-ray holography.

7.9.3 RADIATION TECHNOLOGY Synchrotron radiation opens possibilities in the field of radiation chemistry and technology that have not yet been evaluated. It is possible, for example, that techniques will be developed to modify the surface and bulk properties of materials by irradiation with synchrotron radiation, similar to radiation processes now in use commercially to manufacture "shrink-tubing" for electrical insulation.

With existing storage rings and synchrotrons, photon energies up to 50–100 keV are available for such work. With machines under construction and with wigglers, this could be extended to several hundred keV. Richter (251) has pointed out that a very large (100 GeV) electron storage ring would make available an enormous flux of x rays extending into the MeV range and has suggested that applications such as the sterilization of grain for storage in a worldwide "grain bank" should

be considered. At these high photon energies, the walls of the ring vacuum chamber are transparent, so the radiation emerges from all parts of the orbit without the necessity of installing tangent beam pipes.

7.9.4 MEDICAL APPLICATIONS Using conventional x-ray sources, it has been shown (252–254) that a significant improvement in the contrast of diagnostic x radiographs can be achieved with a technique called dichromatography. In this method, a pair of transmission radiographs are recorded, one below and one above an x-ray absorption edge. The difference between the signals obtained has high sensitivity for the detection of small concentrations of the particular element whose edge has been selected. This could be an aid to early detection of tumors that may have a higher concentration of a particular element than normal tissue. Other applications include improving the sensitivity and reducing the dose to the patient in thyroid dichromatography at the iodine K edge (33 keV).

Synchrotron radiation offers precise tunability and high intensity, which should greatly facilitate dichromatography. The use of improved electronic position-sensitive detectors and associated data storage systems should also be of great benefit in developing the technique. A system for using synchrotron radiation for dichromatography and other medical purposes is briefly described by Kulipanov & Skrinskii (50).

Combining dichromatography with computerized axial tomography (255) might result in contrast and sensitivity improvements beyond that available from either of these techniques alone. The possibility also exists that monochromatic radiation just above the K edge of a particular element might be useful in radiation therapy (50), if the concentration of that element was high enough in the tumor. Such selective absorption could also be the basis of molecular microsurgery (50), the cutting apart of individual molecules at particular locations.

8 CONCLUSION

The extraordinary properties of synchrotron radiation and its rapidly increasing availability throughout the world are having a profound, perhaps revolutionary, impact on a broad range of scientific and technological disciplines. This is all the more remarkable when one realizes that the very substantial results to date, as reviewed in this article, have been accomplished largely symbiotically during high energy physics experimental runs.

With dedicated operation of existing sources and with the design and construction of dedicated storage rings in at least three countries, a

significant increase in experimental capability will soon be realized. Furthermore, there is the exciting promise of enhanced and modified radiation produced by special insertions such as high field standard wiggler magnets, narrow-band interference wigglers, and even narrower-band, tunable, free electron lasers.

The breadth of application of intense synchrotron radiation, extending from the infrared through the visible and ultraviolet parts of the electromagnetic spectrum and deep into the x-ray and soon the γ-ray regions, brings into the same laboratory scientists from diverse specialties such as catalytic chemistry, surface physics, structural biology, and metallurgy. The interchange among these groups during experimental runs or at users' meetings provides added stimulation and enrichment to all, particularly to students just beginning their scientific careers.

It is clear to those of us close to the development of synchrotron radiation research over the past several years that man is now producing electromagnetic radiation in one of nature's most effective ways—witness the crab nebula. The simplicity and efficiency of producing electromagnetic radiation by using relativistic electrons following curved trajectories in an ultra-high vacuum and the scientific appropriateness of this radiation make synchrotron radiation a most elegant, aesthetically pleasing phenomenon.

ACKNOWLEDGMENTS

The task of summarizing scientific work over the vast domain covered here could not have been accomplished without considerable help from those more familiar with specific areas. For aid in writing portions of the manuscript, in finding the relevant literature, and in reviewing drafts, we are indebted to: R. Bachrach, B. Crasemann, P. Csonka, P. Eisenberger, P. Flinn, T. M. Hayes, K. Hodgson, I. Lindau, F. W. Lytle, K. Monahan, W. Parrish, E. M. Rowe, S. Ruby, M. Sauvage, D. Sayers, D. Shirley, W. E. Spicer, E. M. Stern, and J. Stöhr.

The typing and editorial help of Georgia Hathorne have been invaluable. To her we are most indebted.

Literature Cited

1. Averill, R. J., Colby, W. F., Dickenson, T. S., Hofmann, A., Little, R., Maddox, B. J., Mieras, H., Paterson, J. M., Strauch, K., Voss, G.-A., Winick, H. 1973. *IEEE Trans. NS* 20:813–15
2. Koch, E. E., Kunz, C., Weiner, E. W. 1976. *Optik* 45:395–410
3. Koch, E. E., Kunz, C. 1977. *Synchrotronstrahlung bei DESY Ein Handbuch für Benutzer*. 420 pp.
4. Dagneaux, P., Depautex, C., Dhez, P., Durup, J., Farge, Y., Fourme, R., Guyon, P.-M., Jaeglé, P., Leach, S., López-Delgado, R., Morel, G., Pinchaux, R., Thiry, P., Vermeil, C., Wuilleumier, F. 1975. *Ann. Phys.* 9:9–65

5. Hodgson, K. O., Chu, G., Winick, H., eds. 1976. *SSRP Rep. 76/100*
6. Winick, H. 1974. *Proc. Int. Conf. High Energy Accel., 9th*, Stanford, CA, pp. 685–88; Winick, H. 1974. See Ref. 208, pp. 776–80
7. Liénard, A. 1898. *L'Eclairage Elect.* 16:5
8. Jassinsky, W. W. 1935. *J. Exp. Theor. Phys. (USSR)* 5:983; 1936. *Arch. Elektrotechnik.* 30:590
9. Kerst, D. W. 1941. *Phys. Rev.* 60:47–53
10. Ivanenko, D., Pomeranchuk, I. 1944. *Phys. Rev.* 65:343
11. Arzimovitch, L., Pomeranchuk, I. 1945. *J. Phys. (USSR)* 9:267; 1946. *J. Exp. Theor. Phys. (USSR)* 16:379
12. Blewett, J. P. 1946. *Phys. Rev.* 69:87–95
13. Schwinger, J. 1949. *Phys. Rev.* 75: 1912–25
14. Marr, G. V., Munro, I. H., Sharp, J. C. 1972. *Synchrotron Radiat.: A Bibliography DNPL/R24*. Sci. Res. Counc.-Daresbury. 208 pp.; also 1974 *DL/Tm 127*. 95 pp.
15. Ivanenko, D., Sokolov, A. A. 1948. *Dokl. Akad. Nauk SSSR* 59:1551
16. Sokolov, A. A., Klepitov, N. P., Ternov, J. M. 1953. *Dokl. Akad. Nauk SSSR* 89:665
17. Sokolov, A. A., Ternov, I. M. 1955. *Sov. Phys. JETP* 1:227–30; 1957. *Sov. Phys. JETP* 4:396–400; 1964. *Sov. Phys. Dok.* 8:1203–5
18. Sokolov, A. A., Ternov, I. M. 1968. *Synchrotron Radiation*. Pergamon
19. Jackson, J. D. 1975. *Classical Electrodynamics*, Ch. 14. New York: Wiley. 848 pp.
20. Elder, F. R., Gurewitsch, A. M., Langmuir, R. V., Pollack, H. D. 1947. *Phys. Rev.* 71:829–30
21. Ado, I. M., Cherenkov, P. A. 1956. *Sov. Phys. Dokl.* 1:517–19
22. Korolev, F. A., Kulikov, O. F., Yarov, A. S. 1953. *Sov. Phys. JETP* 43:1653
23. Korolev, F. A., Kulikov, O. F. 1960. *Opt. Spectrosc. USSR* 8:1–3
24. Corson, D. A. 1952. *Phys. Rev.* 86: 1052–53; 1953. *Phys. Rev.* 90:748–52
25. Tomboulian, D. H. 1955. *US AEC NP-5803*
26. Tomboulian, D. H., Hartman, P. L. 1956. *Phys. Rev.* 102:1423–47
27. Bedo, D. E., Tomboulian, D. H. 1958. *J. Appl. Phys.* 29:804–9
28. Codling, K., Madden, R. P. 1963. *Phys. Rev. Lett.* 10:516–18; 1964. *Phys. Rev. Lett.* 12:106–8; 1964. *J. Opt. Soc. Am.* 54:268; 1965. *J. Appl. Phys.* 36:830–37
29. Bathov, G., Freytag, E., Haensel, R. 1966. *J. Appl. Phys.* 37:3449
30. Rowe, E. M., Mills, F. E. 1973. *Part. Accel.* 4:211–27
31. Winick, H. 1973. *IEEE Trans. NS* 20(3): 984–88
32. Watson, R. E., Perlman, M. L., eds. 1973. *Res. Appl. Synchrotron Radiat. BNL Rep. 50381*. 192 pp.
33. Lindau, I., Donaich, S., Spicer, W. E., Winick, H. 1975. *J. Vac. Sci. Technol.* (6) 12:1123–27
34. *The Scientific Case for Research with Synchrotron Radiation*. 1975. *Daresbury Rep. DL/SRF/R3*. 32 pp.
35. Blewett, J. P., ed. 1977. *Proposal for a National Synchrotron Light Source, BNL 50595*, Vol. I, pp. 1-1 to 10-1, Vol. II, pp. 1-1 to 4-28
36. *A Proposal for a 1.5 GeV Electron Storage Ring as a Dedicated Synchrotron Source*. 1976. (*Pampus*) *FOM Inst. Rep. 39760*; also *Univ. Technol. Rep. NK-235*, Oct.
37. Morse, R. 1976. *An Assessment of the National Need for Facilities Dedicated to the Production of Synchrotron Radiation 1976*, pp. 1–77. Washington, DC: Solid State Sci. Comm., Natl. Res. Counc.
38. Tigner, M. 1977. *IEEE Trans. NS* 24: 1849–53
39. Cerino, J., Golde, A., Hastings, J., Lindau, I., Salsburg, B., Winick, H., Lee, M., Morton, P., Garren, A. 1977. *IEEE Trans. NS* 24:1003–5
40. *Synchrotron Radiation—A Perspective View for Europe*. 1977. Strasbourg, France: Eur. Sci. Found. 87 pp.
41. Haensel, R., Zimmerer, G. 1976. See Ref. 204, pp. 411–34; Basov, N. G., ed. 1975. *Synchrotron Radiation Proceedings (Trudy) of the PN Lebedev Phys. Inst.*, Vol. 80. Moscou Nauka Press. Transl. Consul. Bur., NY, 1976. 224 pp.
42. Godwin, R. P. 1968. *Springer Tracts in Modern Physics*, Vol. 51. Berlin/New York: Springer. 73 pp.
43. Green, G. K. 1977. *BNL Rep. 50522*. 90 pp.; see also *BNL Rep. 50595*, Vol. II
44. Tsien, R. Y. 1972. *Am. J. Phys.* 40:46–56
45. Larmor, J. 1897. *Philos. Mag.* 44:503
46. Csonka, P. 1978. *Part. Accel.* Vol. 8
47. Hastings, J. B., Kincaid, B., Eisenberger, P. 1977. *BNL Rep. 23353*; also 1978. *Nucl. Instrum. Methods*. 152:167–71
48. Coïsson, R. 1977. *Opt. Commun.* 22: 135–37
49. Mack, R. 1966. *Cambridge Electron Accel. Rep. 1027*. 19 pp.
50. Kulipanov, G. N., Skrinskii, A. N. 1977. *Usp. Fiz. Nauk* 122:369–418 English translation *Sov. Phys. Usp.* 20(7):559–86
51. Rehn, V. 1976. See Ref. 5, pp. 32–34
52. Kincaid, B. 1977. *J. Appl. Phys.* 48: 2684–91

53. Sands, M. 1971. *Proc. Int. Sch. Phys. "Enrico Fermi,"* Course 46, pp. 257–411. New York/London: Academic; also *SLAC Rep. 121*, Nov. 1970
54. Pellegrini, C. 1972. *Ann. Rev. Nucl. Sci.* 22:1–24
55. Sabersky, A. P. 1973. *Part. Accel.* 5: 199–206
56. Lindau, I., Pianetta, P. 1976. See Ref. 204, pp. 372–87
57. Hastings, J. 1976. *J. Appl. Phys.* 48: 1576–84
58. Winick, H., Knight, T., eds. 1977. *Wiggler Magnets SSRP Rep. 77/05.* 138 pp.
59. Winick, H. 1978. *Nucl. Instrum. Methods.* 152:9–15
60. Winick, H. 1976. See Ref. 204, pp. 27–42
61. Trzeciak, W. 1971. *IEEE Trans. NS* 18:213–16
62. Brautti, G., Stagno, V. 1976. *Nucl. Instrum Methods* 135:393
63. Bassetti, M., Cattoni, A., Luccio, A., Preger, M., Tazzari, S. 1977. *LNF Rep. 77/26 (R).* Frascati, Italy. 24 pp.
64. Dahl, P. F., Sampson, W. B. 1975. *BNL Rep. 200/9.* 4 pp.
65. Clee, P., Canliffe, N., Simkin, J., Trowbridge, C. W., Watson, M., 1974. *SRS Rep. 74/64.* Daresbury, Engl.
66. Brunk, W. 1977. See Ref. 58, pp. II41–II44
67. Blewett, J. P., Chasman, R. 1977. *J. Appl. Phys.* 48:2692–98
68. Chu, G. 1976. See Ref. 5, pp. 193–215
69. Motz, H., Thon, W., Whitehurst, R. N. 1953. *J. Appl. Phys.* 24:826–33
70. Hofmann, A. 1978. *Nucl. Instrum. Methods.* 152:17–21
71. Alferov, D. F., Bashmakov, Yu. A., Bessonov, E. G. 1974. *Sov. Phys. Tech. Phys.* 18:1336–39
72. Diambrini Palazzi, G. 1968. *Rev. Mod. Phys.* 40:611–31
73. Milburn, R. H. 1963. *Phys. Rev. Lett.* 10:75–77
74. Alferov, D. F., Bashmakov, Yu. A., Belovintsev, K. A., Bessonov, E. G., Cherenkov, P. A. 1977. *Pisma v JETP.* 26:525–29
75. Coïsson, R. 1977. *IEEE Trans. NS* 24:1681–82; 1977. *Nucl. Instrum. Methods* 143:241–43
76. Sabersky, A. P. 1973. *IEEE Trans. NS* 20:638
77. Madey, J. M. J. 1971. *J. Appl. Phys.* 42:1906–13
78. Elias, L. R., Fairbank, W. M., Madey, J. M. J., Schwettman, H. A., Smith, T. I. 1976. *Phys. Rev. Lett.* 36:717–20
79. Deacon, D. A. G., Elias, L. R., Madey, J. M. J., Ramian, G. J., Schwettman, H. A., Smith, T. I. 1977. *Phys. Rev. Lett.* 38:892–94
80. Colson, W. B. 1976. *Phys. Lett. A* 59:187–90; Hopf, F. A., Meystre, P., Scully, M. O., Louisell, W. H. 1976. *Phys. Rev. Lett.* 37:1342–45; Kwan, T., Dawson, J. M., Lin, A. T. 1977. *Phys. Fluids* 20:581–88; Mayer, G. 1977. *Optics Commun.* 20:200–4
81. Vinokurov, N. A., Skrinskii, A. N. 1977. *Inst. Nucl. Phys.* Novosibirsk, USSR. Preprint 77-59
82. Rehn, V., Jones, V. 1978. *Opt. Eng.* Sept./Oct.
83. Spiller, E. 1976. *Appl. Opt.* 15:2333–38
84. McGowan, J. W., Rowe, E. M., eds. 1976. *Quebec Summer Work. Synchrotron Radiat. Facil., June 1976*
85. *Orsay Conf. Synchrotron Radiat. Instrum. Dev. Sept. 1977. Nucl. Instrum. Methods.* Vol. 152, June 1, 1978. 333 pp.
86. Brown, G., Winick, H., eds. 1978. *Proc. Work. X-Ray Instrum. Synchrotron Radiat. Res. SSRL Rep. 78/04*
87. Brown, F. C., Bachrach, R. A., Lien, N. 1978. *Nucl. Instrum. Methods.* 152:73–79
88. Eberhardt, W., Kalkoffen, G., Kunz, C. 1977. See Ref. 3, pp. 112–19; *Nucl. Instrum. Methods.* 152:81–83
89. Depautex, C., Thiry, P., Pinchaux, R., Pétroff, Y., Lepére, D., Passereau, G., Flamand, J. 1978. *Nucl. Instrum. Methods.* 152:101–2
90. Bachrach, R. Z., Flodstrom, S. A., Schnopper, H. W., Delvaille, J. P. 1977. *Int. Conf. Vac. UV Radiat. Physics, 5th,* Montpellier, France
91. Källne, E., Schnopper, H. W., Delvaille, J. P., Van Speybroeck, L. P., Bachrach, R. Z. 1978. *Nucl. Instrum. Methods.* 152:103–7
92. Pruett, C. 1976. See Ref. 84
93. Sagawa, T. 1976. See Ref. 204, pp. 125–46
94. Hastings, J. 1976. See Ref. 84
95. Beaumont, J. H., Hart, M. 1974. *J. Phys. E* 7:823–29
96. Kincaid, B. 1975. *Synchrotron radiation studies of K-edge x-ray photoabsorption spectra: theory and experiment,* PhD thesis, Stanford Univ., *SSRL Rep. 75/03.* 151 pp.
97. Horowitz, P., Howell, J. 1972. *Science* 178:608–11
98. Howell, J., Horowitz, P. 1975. *Nucl. Instrum. Methods* 125:225–30
99. Brown, G. 1976. See Ref. 84
100. Arndt, U. W., Wonacott, A. J., eds. 1977. *The Rotation Method in Crystallography,* pp. 219–61. Amsterdam: North Holland
101. Cork, C., Fehr, D., Hamlin, R., Vernon, W., Xuong, Ng. H., Perez-Mendez, V. 1974. *J. Appl. Crystallogr.* 7:319–23; Cork, D., Hamlin, R., Vernon, W.,

Xuong, Ng. H., Perez-Mendez, V. 1975. *Acta Crystallogr. A* 31:702–3
102. Charpak, G., Hajduk, A., Jeavons, A., Stubbs, R., Kahn, R. 1974. *Nucl. Instrum. Methods* 122:307–12; Charpak, G., Demierre, C., Kahn, R., Santiard, J. C., Sauli, F. 1977. *IEEE Trans. NS* 24(1):200–4
103. Ederer, D. L., Saloman, E. B., Ebner, S. C., Madden, R. P. 1975. *J. Res. Natl. Bur. Stand.* 79A:761
104. Schnopper, H. W., Van Speybroeck, L. P., Delvaille, J. P., Epstein, A., Källne, E., Bachrach, R. Z., Dijkstra, J. H., Lantward, L. 1977. *Appl. Opt.* 16:1088–91
105. Norem, J. H., Young, K. M. 1977. *Argonne Natl. Lab. ANL/FPP Tech. Memo.* 79
106. Stevenson, J. R., Ellis, H., Bartlett, R. 1973. *Appl. Opt.* 12:2884–89
107. James, R. W. 1962. *The Optical Principles of the Diffraction of X-rays*, Ch. 4. London: Bell
108. Ramaseshan, S., Abrahams, S. C., eds. 1975. *Anomalous Scattering*. Copenhagen: Munksgaard. 539 pp.
109. Phillips, J. C., Wlodawer, A., Goodfellow, J. M., Watenpaugh, K. D., Sieker, L. C., Jensen, L. H., Hodgson, K. O. 1977. *Acta Crystallogr. A* 33: 445–55
110. Phillips, J. C., Wlodawer, A., Yevitz, M. M., Hodgson, K. O. 1976. *Proc. Natl. Acad. Sci. USA* 73:128–32
111. Guttman, L., 1956. *Solid State Phys.* 3:146–223
112. Keating, D. T. 1963. *J. Appl. Phys.* 34:923–25
113. Bienenstock, A. 1977. In *The Structure of Non-Crystalline Materials*, ed. P. H. Gaskell, pp. 5–11. London: Taylor & Francis. 262 pp.
114. Waseda, Y., Tamaki, S. 1975. *Philos. Mag.* 32:951; and 1976. *Z. Phys. B* 23
115. Fuoss, P., Bienenstock, A. 1976. *Bull. Am. Phys. Soc.* 22:405
116. Shevchik, N. 1977. *Philos. Mag.* 35: 805–9, 1289–98
117. Bonse, U., Materlik, G. 1976. *Z. Phys. B* 24:189–91
118. Bonse, U., Materlik, G. 1975. See Ref. 108, pp. 107–9
119. Fukamachi, T., Hosoya, S., Kawamura, T., Hastings, J. 1977. *J. Appl. Crystallogr.* 10:321
120. Barrington Leigh, J., Rosenbaum, G. 1976. *Ann. Rev. Biophys. Bioeng.* 5: 239–70
121. Bordas, J., Munro, I. H., Glazer, A. M. 1976. *Nature* 262:541–45
122. Blaurock, A. E. 1978. *Biochim. Biophys. Acta*. In press
123. Webb, N. G. 1976. *Rev. Sci. Instrum.* 47:545–47
124. Buras, B., Olsen, J. S., Gerward, L. 1976. *Nucl. Instrum. Methods* 135: 193–95
125. Bordas, J., Glazer, A. M., Howard, C. J., Bourdillon, A. J. 1977. *Philos. Mag.* 35:311–23
126. Tuomi, T., Naukkarinen, K., Rabe, P. 1974. *Phys. Status Solidi A* 25:93
127. Hart, M. 1975. *J. Appl. Crystallogr.* 8:436
128. Bordas, J., Glazer, A. M., Hauser, H. 1975. *Philos. Mag.* 32:471
129. Tanner, B. K., Safa, M., Midgley, D., Bordas, J. 1976. *J. Magn. Mater.* 1:337; Tanner, B. K., Safa, M., Midgley, D. 1977. *J. Appl. Crystallogr.* 10:91
130. Miltat, J. 1978. *Nucl. Instrum. Methods.* 152:323–29
131. Steinberger, I. T., Bordas, J., Kalman, Z. H. 1977. *Philos. Mag.* 35:1257
132. Petroff, J. F., Sauvage, M. 1978. *J. Cryst. Growth*. In press
133. Ruby, S. L. 1974. *J. Phys. C* 6:209
134. Perlow, G. J., ed. 1977. *Workshop on New Directions in Mössbauer Spectroscopy, Argonne 1977*. Am. Inst. Phys. Conf. Proc. 38, p. 46, 91, 140
135. Hunter, S. H. 1977. *A structural study of amorphous copper-arsenic triselenide alloys using EXAFS*, PhD thesis, Stanford Univ.; *SSRL Rep. 77/04*. 136 pp.
136. Lytle, F. W. 1965. In *Physics of Non-Crystalline Solids*, ed. J. A. Prins, pp. 12–29. Amsterdam: North Holland
137. Lytle, F. W. 1966. In *Advances in X-ray Analysis*, ed. G. R. Mallett, M. J. Fay, W. M. Mueller, Vol. 9, pp. 398–409. New York: Plenum
138. Sayers, D. E., Lytle, F. W., Stern, E. A. 1970. In *Advances in X-ray Analysis*, ed. B. L. Henke, J. B. Newkirk, G. R. Mallett, Vol. 13, pp. 248–71. New York: Plenum
139. Sayers, D. E., Stern, E. A., Lytle, F. W. 1971. *Phys. Rev. Lett.* 27:1204–7
140. Ashley, C. A., Doniach, S. 1975. *Phys. Rev. B* 11:1279–88
141. Lytle, F. W., Sayers, D. E., Stern, E. A. 1977. *Phys. Rev. B* 15:2426–28
142. Knights, J. C., Hayes, T. M., Mikkelsen, J. C. Jr. 1977. *Phys. Rev. Lett.* 39: 712–15
143. Lee, P. A., Beni, G. 1977. *Phys. Rev. B* 15:2862–83
144. Lee, P. A., Pendry, J. B. 1975. *Phys. Rev. B* 11:2795–2811
145. Rehr, J. J., Stern, E. A. 1976. *Phys. Rev. B* 14:4413–19
146. Kincaid, B. M., Eisenberger, P. 1975. *Phys. Rev. Lett.* 34:1361–64

147. Kincaid, B. M. 1975. See Ref. 96, Ch. 3
148. Citrin, P. H., Eisenberger, P., Kincaid, B. M. 1976. *Phys. Rev. Lett.* 36:1346–49
149. Lee, P. A., Teo, B. K., Simons, A. L. 1977. *J. Am. Chem. Soc.* 99:3856–57
150. Teo, B. K., Lee, P. A., Simons, A. L., Eisenberger, P., Kincaid, B. M. 1977. *J. Am. Chem. Soc.* 99:3854–55
151. Hayes, T. M., Sen, P. N., Hunter, S. H. 1976. *J. Phys. C* 4357
152. Hayes, T. M., Sen, P. N., Hunter, S. H. 1976. In *Structure and Excitations of Amorphous Solids*, ed. G. Lucovsky, F. L. Galeener, pp. 166–171. New York: AIP. 403 pp.
153. Stern, E. A., Sayers, D. E., Lytle, F. W. 1975. *Phys. Rev. B* 11:4836–46
154. Hunter, S. H., Bienenstock, A., Hayes, T. M. 1977. See Ref. 113, pp. 73–76
155. Cramer, S. P., Eccles, T. K., Kutzler, F., Hodgson, K. O., Doniach, S. 1976. *J. Am. Chem. Soc.* 98:8059–69
156. Watenpaugh, K. D., Sieker, L. C., Heriott, J. R., Jensen, L. H. 1973. *Acta Crystallogr. B* 29:943
157. Shulman, R. G., Eisenberger, P., Blumberg, W. E., Stombaugh, N. A. 1975. *Proc. Natl. Acad. Sci. USA* 72:4003–7
158. Bunker, B., Stern, E. A. 1977. *Biophys. J.* 19:253–64
159. Sayers, D. E., Stern, E. A., Herriot, J. R. 1976. *J. Chem. Phys.* 64:427
160. Shulman, R. G., Eisenberger, P., Teo, B. K., Kincaid, B. M., Brown, G. S. 1978. *J. Mol. Biol.* In press
161. Eisenberger, P., Shulman, R. G., Brown, G. S., Ogawa, S. 1976. *Proc. Natl. Acad. Sci. USA* 73:491–95
162. Sayers, D. E., Lytle, F. W., Weissbluth, M., Pianetta, P. 1975. *J. Chem. Phys.* 62:2514–15
163. Kincaid, B. M., Eisenberger, P., Hodgson, K. O., Doniach, S. 1975. *Proc. Natl. Acad. Sci. USA* 72:2340–42
164. Hu, V. W., Chan, S. I., Brown, G. S. 1977. *Proc. Natl. Acad. Sci. USA* 74:3821–25
165. Cramer, S. P., Hodgson, K. O., Stiefel, E. I., Newton, W. E. 1978. *J. Am. Chem. Soc.* 100:2748
166. Cramer, S. P., Hodgson, K. O., Gillum, W. O., Mortenson, L. E. 1978. *J. Am. Chem. Soc.* 100:11
167. Cramer, S. P., Gillum, W. O., Hodgson, K. O., Mortenson, L. E., Stiefel, E. I., Chisnell, J. R., Brill, W. J., Shah, V. K. 1978. *J. Am. Chem. Soc.* 100:3398–3407
168. Sayers, D. E., Lytle, F. W., Stern, E. A. 1972. *J. Non-Cryst. Solids* 8–10:401–7
169. Sayers, D. E., Lytle, F. W., Stern, E. A. 1974. In *Amorphous and Liquid Semiconductors*, ed. J. Stuke, W. Brenig, Vol. I, p. 403–12. London: Taylor & Francis. 735 pp.
170. Bienenstock, A., Mortyn, F., Narasimhan, S., Rowland, S. C. 1976. In *Frontiers in Materials Science—Distinguished Lectures*, ed. L. Murr, C. Stein, pp. 1–18. New York: Dekker. 590 pp.
171. Mott, N. F. 1967. *Adv. Phys.* 16:49–144
172. Hunter, S., Bienenstock, A. 1976. In *Structure and Properties of Non-Crystalline Semiconductors*, ed. B. T. Kolomiets, pp. 151–54. Leningrad: Ioffe Phys.-Tech. Inst. 546 pp.
173. Hunter, S. H., Bienenstock, A., Hayes, T. M. 1977. In *Amorphous and Liquid Semiconductors*, ed. W. E. Spear, pp. 78–82. Univ. Edinburgh. 891 pp.
174. Crozier, E. D., Lytle, F. W., Sayers, D. E., Stern, E. A. 1977. *Can. J. Chem.* 55:1968–74
175. Lytle, F. W., Sayers, D. E., Moore, E. B. Jr. 1974. *Appl. Phys. Lett.* 24:45–47
176. Bassi, I. W., Lytle, F. W., Parraveno, G. 1976. *J. Catal.* 42:139–47
177. Lytle, F. W., Via, G. H., Sinfelt, J. H. 1977. *J. Chem. Phys.* 67:3831–32
178. Reed, J., Eisenberger, P., Teo, B. K., Kincaid, B. M. 1977. *J. Am. Chem. Soc.* 99:5217–18
179. Reed, J., Eisenberger, P. 1977. *J. Chem. Soc. Chem Commun.* 18:628–30
180. Sinfelt, J. H., Via, G. H. Lytle, F. W. 1978. *J. Chem. Phys.* 68:2009
181. Lytle, F. W. 1976. *J. Catal.* 43:376–79
182. Stern, E. A., Sayers, D. E., Dash, J. G., Shechter, H., Bunker, B. 1977. *Phys. Rev. Lett.* 38:767–70
183. Stern, E. A. 1977. *J. Vac. Sci. Technol.* 14:461–65
184. Lee, P. A. 1976. *Phys. Rev. B* 13:5261–70
185. Citrin, P. H., Eisenberger, P., Hewitt, R. C., Schwartz, G. 1977. Presented at Ann. Stanford Synchrotron Lab. Users Group Meet., 4th, Stanford, CA
186. Jaklevic, J., Kirby, J. A., Klein, M. P., Robertson, A. S., Brown, G. S., Eisenberger, P. 1977. *Solid State Commun.* 23:679–82
187. Sparks, C. J., Raman, S., Yakel, H. L., Gentry, R. V., Krause, M. O. 1977. *Phys. Rev. Lett.* 38:205–8
188. Sparks, C. J., Raman, S., Ricci, E., Gentry, R. V., Krause, M. O. 1978. *Phys. Rev. Lett.* 40:507–11
189. Gentry, R. V. 1976. *Phys. Rev. Lett.* 37:11
190. Ilin, V. A., Kazakevich, G. M., Kulipanov, G. N., Mazalov, L. N., Matyushin, A. M., Skrinskii, A. N., Sheromov, M. A. 1977. *Nucl. Phys.*

Inst., Novosibirsk, USSR. Preprint 77-13
191. Spears, D. L., Smith, H. I. 1972. *Electron. Lett.* 8:102–4; *Solid State Technol.* 15:21–26
192. Spiller, E., Eastman, D. E., Feder, R., Grobman, W. D., Gudat, W., Topalian, J. 1976. *J. Appl. Phys.* 47:5450–59
193. Fay, B., Trotel, J., Petroff, Y., Pinchaux, R., Thiry, P. 1976. *Appl. Phys. Lett.* 29:370–72
194. Spiller, E., Feder, R. 1977. *Topics in Applied Physics*, ed. H. J. Queisser, Vol. 22, pp. 35–92. New York: Springer
195. Robinson, A. 1978. *Science* 199:411–13
196. Koronkevich, V. P., Kulipanov, G. N., Nalivaiko, V. I., Pindyurin, V. F., Skrinskii, A. N. 1977. *Nucl. Phys. Inst.*, Novosibirsk, USSR. Preprint 77-10
197. Sayre, D., Kirz, J., Feder, R., Kim, D. M., Spiller, E. 1977. *Science* 196: 1339–40
198. Kirz, J., Sayre, D., Dilger, J. 1977. See Ref. 197
199. Horowitz, P., Aronson, M., Grodzins, L., Ladd, W., Ryan, J., Merriam, G., Lechene, C. 1976. *Science* 194:1162–65
200. Niemann, B., Rudolf, D., Schmahl, G. 1976. *Appl. Opt.* 15:1883–84
201. Feder, R., Spiller, E., Topalian, J., Broers, A. N., Gudat, W., Panessa, B. J., Zadunaisky, Z. A. 1977. *Science* 197:259–60
202. Polack, F., Lowenthal, S., Petroff, Y., Farge, Y. 1977. *Appl. Phys. Lett.* 31:785–87
203. Haensel, R., Kunz, C. 1967. *Z. Angew. Phys.* 23:276
204. Mancini, A. N., Quercia, I. F., eds. 1976. *Int. Coll. Appl. Phys. Inst. Naz. Fis. Nucl. Course Synchrotron Radiation*, Vol. I, 481 pp., Vol. II, 84 pp.
205. Sokolov, A. A., Ternov, J. M. 1968. *Synchrotron Radiation.* Oxford: Pergamon. 207 pp. (from Russian)
206. Codling, K. 1973. *Rep. Progr. Phys.* 36:541
207. Brown, F. C. 1974. In *Solid State Physics*, ed. H. Ehrenreich, F. Seitz, D. Turnbull, 29:1–73. New York: Academic. 388 pp.
208. Koch, E. E., Haensel, R., Kunz, C., eds. 1974. *Vacuum Ultraviolet Radiation Physics*, Braunschweig: Vieweg/ Pergamon. 832 pp.
209. Haensel, R. 1975. In *Festkörperprobleme, Advances in Solid State Physics*, ed. H. J. Queisser, 15:203–28. Braunschweig: Pergamon
210. Koch, E. E., Otto, A. 1976. *Int. J. Radiat. Phys. Chem.* 8:113
211. Kunz, C. 1976. In *Optical Properties of Solids—New Developments*, ed. B. O. Seraphin, p. 473. Amsterdam: North-Holland
212. Sonntag, B. 1976. In *Rare Gas Solids*, ed. M. L. Klein, J. A. Venables, Vol. 2. New York: Academic
213. Koch, E. E., Kunz, C., Sonntag, B. 1977. *Phys. Rep.* 29:153–231
214. Spicer, W. E. 1978. In *Electron and Ion Spectroscopy of Solids*, pp. 54–89
215. Shirley, D. A., Stöhr, J., Wehner, P. S., Williams, R. S., Apai, G. 1978. *Phys. Scr.* 16:398–413
216. Lynch, D. W. 1976. See Ref. 204, pp. 26–85
217. Aspnes, D. A. See Ref. 204, pp. 286–97
218. Mahan, G. D. 1974. See Ref. 207, pp. 75–138
219. Cooper, J. W. 1964. *Phys. Rev. Lett.* 13:762–64
220. Fano, U., Cooper, J. W. 1968. *Rev. Mod. Phys.* 40:441–507
221. Wehner, P. S., Stöhr, J., Apai, G., McFeely, F. R., Williams, R. S., Shirley, D. A. 1976. *Phys. Rev. B* 14:2411–16
222. Stöhr, J., Apai, G., Wehner, P. S., McFeely, F. R., Williams, R. S., Shirley, D. A. 1967. *Phys. Rev. B* 14:5144–55
223. Lindau, I., Pianetta, P., Spicer, W. E. 1976. *Phys. Lett. A* 57:225–26
224. Lindau, I., Pianetta, P., Spicer, W. E. 1978. In *Proc. Int. Conf. Phys. X-ray Spectra, 1976*, ed. R. D. Deslattes, p. 78.
225. Eastman, D. E. 1974. See Ref. 208, p. 417
226. Lindau, I. 1976. See Ref. 204, pp. 319–71
227. Lindau, I., Spicer, W. E. 1974. *J. Electron. Spectrosc.* 3:409
228. Rowe, E. M., ed. 1977. *Notes on the Annual Synchrotron Radiation Users Group Conference*, The Synchrotron Radiation Center, Stoughton, WI
229. Brown, G. S., ed. 1977. *Ann. Stanford Synchrotron Radiat. Lab Users Group Meet., 4th, SSRL Rep. 77/11*, Stanford. 75 pp.
230. López-Delgado, R., Tramer, A., Munro, I. H. 1974. *Chem. Phys.* 5:72
231. Lindquist, L., López-Delgado, R., Martin, M. M., Tramer, A. 1974. *Opt. Commun.* 10:283–87
232. Benoist D'Azy, O., López-Delgado, R., Tramer, A. 1975. *Chem. Phys.* 9:327
233. López-Delgado, R., Miehé, J. A., Sipp, B. 1976. *SSRL Rep. 76/04.* 10 pp.
234. López-Delgado, R. 1976. See Ref. 204, pp. 63–124
235. Monahan, K. M., Rehn, V. 1978. *Nucl. Instrum. Methods.* 152:255–59
236. Matthias, E., Rosenberg, R. A., Poliakoff, E. D., White, M. G., Lee,

S.-T., Shirley, D. A. 1977. *Chem. Phys. Lett.* 52:239
237. Matthias, E., White, M. G., Poliakoff, E. D., Rosenberg, R. A., Lee, S.-T., Shirley, D. A. 1978. *Chem. Phys. Lett.* 54(1):30–34
238. Monahan, K. M., Rehn, V., Matthias, E., Poliakoff, E. 1977. *J. Chem. Phys.* 67:1784–86
239. Monahan, K. M., Rehn, V. 1977. *SSRL Rep. 77/10*
240. Monahan, K. M. 1978. *Bull. Am. Phys. Soc.* 23:61
241. Hahn, U., Jordan, B., Schwentner, N. 1977. *Extended Abstr. Int. Conf. Vac. Ultraviolet Radiat. Phys., 5th,* 3:202, Montpellier, France
242. Ice, G. E., Chen, M. H., Crasemann, B. 1978. *Phys. Rev. A* 17:650
243. Bentley, J. J., Stewart, R. F. 1975. *J. Chem. Phys.* 62:875–78
244. Csonka, P. 1977. *SSRL Rep. 77/03*; Csonka, P., Crasemann, B. 1975. *Phys. Rev. A* 12:611–14; Csonka, P. 1977. *Phys. Rev. A* 13:405–10; Univ. Ore. *Preprint ITS NT 065/77*
245. Kondratenko, A. M., Skrinskii, A. N. 1977. *Opt. Spectrosc.* 42:189–92
246. Kikuta, S., Aoki, S., Kosaki, S., Kohra, K. 1972. *Opt. Commun.* 5:86–89
247. Aoki, S., Ichihara, Y., Kikuta, S. 1972. *Jpn. J. Appl. Phys.* 11:1857
248. Aoki, S., Kikuta, S. 1974. *Jpn. J. Appl. Phys.* 13:1385–92
249. Csonka, P. 1977. Univ. Ore. Inst. Theor. Stud. *Preprint N.T.* 066/77
250. Csonka, P. 1978 *Part. Accel.* 8:161
251. Richter, B. 1976. *Nucl. Instrum. Methods* 136:47–60
252. Jacobson, B. 1964. *Am. J. Roentgenol. Radium Ther. Nucl. Med.* 91:202
253. Atkins, H. L., Hauser, W., Kraner, H. W. 1972. *Am. J. Roentgenol. Radium Ther. Nucl. Med.* 114:176
254. Mistretta, C. A., Ort, M. G., Kelcz, F., Cameron, J. R., Siedband, M. P., Crummy, A. B. 1973. *Invest. Radiat.* 8:402
255. Swindell, W., Barrett, H. H. 1977. *Phys. Today* 30:32–41
256. Hatzakis, M. 1971. *Appl. Phys. Lett.* 18:7–10
257. Plummer, E. W., Gustafsson, T. 1977. *Science* 198:165–70